The Light Source in High-Voltage Photography

By

William A. Tiller

A. Introduction

We have all been excited and thrilled by the beautiful Kirlian photographs we have seen and are understandably elated by what we think they may portend about the nature of the universe[1,2]. However, after a year or two's experience with high-voltage photography in the United States, it is now time to ask ourselves some serious questions concerning the process: (a) Does the evidence show that we are dealing here with physical or what we might for the moment call non-physical effects? (b) Can we realistically account for the observations made to date with a specific model? (c) Are we doing our experiments carefully enough to continue making meaningful progress? The present paper speaks to these questions and concludes that: (a) There is a specific physical explanation, called the streamer phenomenon of corona discharge, that can account for all the observations made to date. (b) The identification of a specific physical mechanism does not mean that energy interactions with non-physical levels may not be intimately involved. (c) We are definitely not

conducting our experiments carefully enough to make rapid and meaningful progress.

To begin this exposition, let us briefly discuss the author's model of the non-physical aspects of the universe so that our frame of reference will have been at least identified and understood (even if not accepted)[3].

B. Model of Radiation and Substance

In order to provide a slight background perspective of radiators, absorbers, and radiation, the simplest place to begin is at the level of the atom. A simple model of the atom is that of a nucleus of positive charge surrounded by a number of electrons, each of them being in well-defined but different energy states. Other possible states for these electrons exist but, in the atom's equilibrium state, they are not filled by electrons. If we stimulate the atom, we can cause the electrons to shift to these unfilled or excited levels and, when they drop back into their equilibrium levels, they emit electromagnetic (E.M.) radiation which is often in the visible range of the E.M. spectrum. In Fig. 1, some of these energy levels are schematically illustrated using the simple Bohr model for the hydrogen atom.

A useful model for simulating the behavior of the electron level changes is the "classical harmonic oscillator". We say that a charged particle of mass M is bound to a position of equilibrium with a spring by a force of interaction G (known as the force constant of the spring) as illustrated in Fig. 2. When the particle is displaced from its equilibrium position and released, it is found to vibrate at its resonant frequency ν_o given by

$$\nu_o = \frac{1}{2\pi}\left(\frac{G}{M}\right)^{\frac{1}{2}} \qquad (1)$$

and the amplitude decays with time because of the frictional damping in the spring; i.e., it acts something like the familiar tuning fork. For the charged

particle, the initial displacement may be caused by the exchange of energy with another atom or by the absorption of some electromagnetic energy.

This provides us with a very simple model of a light source. The vibrating charge will create an electromagnetic field oscillating in a narrow frequency range $\Delta\nu$ about the resonant frequency as illustrated in Fig. 3. Here, $I(\nu)$ is the intensity of the radiation from the source at frequency ν. In general, a given type of atom will exhibit a spectrum of such frequencies, i.e., a series of such lines at different frequencies where each line is associated with an electron transition from one orbital energy level to another.

If we consider groups of identical atoms, the foregoing describes the situation so long as the atoms are far apart and isolated from each other. They give identical spectra with lines of the type illustrated in Fig. 3. If we allow two of these atoms to come closer together so that they begin to exert a force on each other (an electrostatic force), they become coupled so that G in Fig. 2 is no longer a constant; i.e., the motion of one exerts a force on the other. For these two atoms, their resonant frequency changes from one value, ν_o, to two values, ν_1 and ν_2, which depends upon the distance of separation of the atoms as illustrated in Fig. 4. The values of ν_1 and ν_2 diverge from each other as the atoms become closer and closer together and interact with a tighter coupling. We complete the picture by considering many atoms interacting very strongly with each other. This provides a whole range of overlapping resonant frequencies which cause the simple resonant line of Fig. 3 to broaden into the resonant band of Fig. 5.

Before we press on, there are a variety of important characteristics that we should note concerning these electronic vibrational states of matter. First, every atom, molecule, cell, gland, animal, etc., has at least one resonant

energy band of some bandwidth $\Delta\nu$ at which it will both emit energy (E.M. radiation) in some spatial pattern and absorb it; i.e., they are both the same for a particular system. Thus, each system is in communication with the outside world (transmitting and receiving) via its resonant frequency spectrum. This particular spectrum is like a unique fingerprint via which we can identify the system.

If we look carefully at the human body with electromagnetic detectors, we are able to see E.M. energy radiated from the body not only as a result of electron orbit changes but also as a result of physical rotations and vibrations of the molecules, cells, etc. In time, we may even come to detect natural X-ray and γ-ray emission from certain regions of the body. In addition, if we carefully scan the body with sonic detectors, we shall detect a unique sound spectrum associated with actual physical movement of cells and body systems--another fingerprint. In time, we can expect to find many such fingerprints radiated from the physical body.

Perhaps one of the most striking techniques for revealing some of these energies is the use of liquid crystals. By painting a person's body with liquid crystals, color patterns can be readily seen. Here, the liquid crystal acts as a transducer to turn the body's radiations into an optical manifestation that can be readily seen.

These are the types of radiation we know at this point in time, and we are trying to use this as a guideline for understanding the uncommon energies we hear about. We hear of psychometry. We hear of dowsing. We hear of clairvoyance and clairaudience and prophecy and various kinds of channeling activities. We hear about radionics, vivaxis, and many other nonconventional methods of gaining information about our environment and about ourselves. You see, we communicate with each other only through radiation patterns and

although we think conventionally in terms of the visual (which is electromagnetic) and in terms of the sonic, we should antitipate that nature is filled with many, many other kinds of energies. As we attune to them and discriminate them, then we, in fact, are obtaining additional information about our environment.

Let us now extend these radiation ideas to substances from other dimensions of the universe than the physical. Starting with the yogic philosophy of the seven principles operating in man, I hypothesize that this means there are really seven different levels of substance in the universe and that these different substances have different types of configurations. They obey entirely different kinds of laws--unique types of laws--and they have unique characteristics of radiation (absorption and emission). I further postulate that they operate in different kinds of space-time frames in the universe and so are distinct from each other. The seven levels of substance, then, from the coarsest going towards the finest are: (1) the physical level that we are familiar with; (2) the etheric level (the Russians call this the bioplasmic body or the energy body; some people call it the prephysical body); (3) the astral level; (4) there are three levels of mind: instinctive, intellectual, and spiritual mind; and (5) another distinct level, which is spirit.

There is considered to be a level beyond these seven which shall be called the Divine. However, relative to all that I think we will be capable of perceiving for a very long period in the course of human evolution, we may think just in terms of the seven levels of substance.

These seven substances interpenetrate each other in nature and may interact with each other. They, through the polarity principle, form atoms and molecules and configurations of these. One can apply the metaphysical principle: "As

above, so below; as below, so above," and realize that what we see in the physical may be used as a model and this same kind of modelling understanding may be extrapolated through the other levels of substance, differing somewhat in detail from the physical, and we may begin conceptually to grapple with these other levels. The substances interpenetrate, and their relationship may be visualized by considering the situation in our own bodies. To visualize our seven bodies, think of seven transparent sheets of paper and, on these sheets, using particular pens of different colors, draw circuitry of one color on one, and on another draw circuitry of another color, and so on through the seven colors. Then, put these sheets all together and look through them, and you will see an organization of substance at the various levels within the bodies of man. That, basically, is the model I wish to project.

In general, these substances do not interact with each other too strongly. However, they can be brought into interaction with each other through the agency of mind, and it is really at the point of mind that one can bring about changes in the organization of structure in these various levels of substance. That is, through mind forces, one can create a pattern, and that pattern then acts as a force field which applies to the next level of substance. In turn, that force field is a force for organizing the atoms and molecules into configurations at that level of substance. That pattern of substance at the etheric level, then, is in a particular state of organization and it has its own radiation field--its own force field, if you like--and that force field, then, is a field for the organization of matter at the next level of substance --the physical level of substance. These etheric forces, then, bring about the coalescence and organization of matter at the physical level of substance.

Here, we see something that I have chosen to call the "ratchet" effect; one can see an action beginning at the mind level and working its way down

through to produce an effect on the physical level (and vice versa).

As an aid to visualizing this model, consider Fig. 6. For these seven levels of substance it is meaningful to draw a plot of the intensity of the radiation versus its frequency. Now, the thing we have to realize is that this particular representation of Fig. 6 is purely for coming into contact with the idea and is not a scientifically correct representation, since these levels of substance represent entirely different kinds of energy, entirely different kinds of physical laws, and they really should be represented on different axes, i.e., different coordinate vectors of phase space. That would be a more proper way to do it. And, in fact, along any one of these coordinates, there may be many different kinds of energy that should be represented (just like electromagnetic, sonic, gravity, etc., energies in the physical). But, at least for us to conceptually see the simplest outlines of the model, it is worthwhile to represent it this way: the physical, etheric, astral, mind levels and the spiritual level on one axis. Through focusing attention on the mind and spirit levels, here we see the true essence of man. This is the indestructible reality of man and is the on-going man. These levels of energy function (or appear to function) in a non-space, non-time frame of reference--that is, the patterns of intelligence (in that frame of reference) are not represented on coordinates which relate to space and time.

The astral function is largely as a containment vehicle, it appears, to keep this human essence in a compact form between incarnations. It is also considered to be the energy construct of our emotional body. Looking further to the left, we come down to the temporal reality associated with this kind of physical existence, i.e., a vehicle that is suitable for experience in this earth plane (the etheric level and the physical level). In the case of the physical, we have the space-time frame which is the Einsteinian frame which

we know a great deal about. The etheric level is a companion level and it operates again in a space-time frame but in a different space-time frame from the physical, and yet these two are complementary. That is, as time goes on, for the physical, the potential decreases and entropy increases, whereas for the etheric we have the reverse situation (the potential increases and entropy decreases). A characteristic of the physical frame is one of disorder. A characteristic of the etheric frame is one of the organization of matter. The physical is primarily characterized by electric effects. The etheric is primarily characterized by magnetic effects. In the physical, mass and time are positive; in the etheric they are negative. Considering Fig. 7, if we increase the velocity of a physical particle, its energy is predicted to increase towards infinite values as its velocity approaches the speed of light (theory of relativity). However, although $v = c$ is a mathematical singularity, the behavior will be like most physical processes and, at a sufficiently small difference of v from c, the particle will tunnel through the energy barrier leaving the physical domain and find itself transformed into the etheric domain with a large negative energy. Perhaps we see here an idea that relates to "quasars" and "black holes in space." In any event, by definition, a particle with velocity greater than c is called non-physical (tachyons for electromagnetic particles) and that is why we use the term in this section.

This is the way in which I have come to look at these various energies; i.e., that there are radiations associated with these different levels, and these radiations give rise to the phenomena that we can call psychoenergetics. The majority of these phenomena deal with the etheric vehicle. That is, we have a sensory system in this vehicle which connects us to the psychoenergetic phenomena just as our five physical senses connect us to physical phenomena.

C. Rational Experimental Expectations

Using our five physical senses and an army of instruments based on similar reference frame experience, we discriminate information patterns radiated to us by reality. We cannot expect to "know" reality but can only ask for consistency amongst the many information patterns we perceived concerning reality[3]. Following this line, suppose we seek to discriminate information patterns radiated to us by Nature but on a non-physical band rather than on a physical band. We will find that the phenomenon which we think is non-physical will influence our physical observations in some way and we will eventually come upon a physical explanation. This should not be too surprising to us because all we can presently perceive, with any reliability, is a physical manifestation of energy and there must be a perfectly logical mechanism and physical explanation for the process of its appearance and registration by our senses. It is thus necessary to understand the physical process to such an extent that one can track its roots backwards to some causal and non-random event that strongly suggests non-physical connections. An information pattern at a non-physical level will act as a force field with coupling elements to the physical dimension so that a corresponding (not necessarily same shape or intensity) force field pattern will be mapped (or transduced) into the physical level which, in turn, sets a physical process in motion which we then observe with our physical instruments.

As an example, we might take the phenomenon of psychokinesis. A subject projects a non-physical energy pattern to an object located in a Faraday cage. The object lifts and translates but we can detect no energy manifestation with our sensors anywhere outside the cage (except in the brainwave, neural, etc. patterns of the subject). Eventually, we may decide to look inside the

cage with electromagnetic and gravity sensors in the immediate vicinity of the object and may locate a divergence of E.M. or gravity field, or both. Thus we see that the final physical manifestation (as determined by our sensate observation instruments) is rationally explained in terms of known physical forces. However, we must be honest and recognize a non-physical energy link in the total causal

D. The Stanford Experiments

Mr. D. Boyers and the author have conducted a number of experiments with the apparatus of Fig. 8[4]. Figure 9 presents a schematic of the Oudin coil. Using short (~ 100 μsec) pulses of R.F. (1 MHz) applied to parallel electrodes in air at small electrode spacings (~ 250 microns) and at an applied field ~ 10^6 volts/cm, discharges from both biological and metallic electrodes were found to occur from a network of points in the electrode surface. These discharges were recorded photographically on a film placed within the electrode space. Multiple pulses were found to produce a superposition effect such that a uniform corona exposure appeared on the film. Figure 10 illustrates the effect of single and multiple pulses for both a coin and a finger tip. The clear delineation of all sharp edges on the coin indicates enhanced field emission of electrons from regions of small radius of curvature. The multiple pulses with the finger electrode led to the familiar halo-like pattern.

During the finger tip studies, it was found that the photograph depended significantly on the orientation and spacing of the finger on the electrode-film combination. Considerable variability occurred in these results as a consequence of the inability to repeatedly establish a well-defined and controlled discharge spacing, the orientation and tilt of the finger plus other

unknown factors. This was especially true with the multiple pulse technique. In order to gain some reliable information, discharges between flat, polished, metal electrodes were investigated.

Figure 11 is a representative photograph of the results with brass. All the photographs were found to reveal the same characteristic dot discharge pattern with relatively uniform dot spacing. The general trends noted in the study were the following: (1) For a given electrode material, increased pulse width increased the dot intensity. (2) For a given pulse width and electrode material, multiple pulses resulted in a decrease in the average inter-dot spacing. (3) For a given pulse width and approximately constant electrode spacing, the inter-dot spacing, λ, varied only slightly from material to material even though their electron work functions differed by as much as two volts. (4) For a given material, increasing electrode spacing results in less discrete dots but produced dot clustering and an increase in the amount of diffuse exposure around each dot. (5) For laterally displaced electrodes (relative to each other) giving only a fractional matching area of electrode, the shape of the discharge not only conforms to the shape of the overlap area but one sees an additional edge discharge from the upper edge that overlies the metal on the lower electrode. (6) In a number of photographs, large clear patches containing no dots were found. This effect disappeared when photographic plates instead of film was used.

One has only to casually read the work of Loeb[5] to realize that we are dealing here with the corona discharge phenomena called "streamers". Since this phenomenon will be discussed at length in the next section, we shall deal with it only briefly here.

A few electrons are produced in the interelectrode space either by cosmic ray events, U.V. radiation, or field emission from the cathode. These

electrons are accelerated by the field and ionize the air molecules yielding an exponential growth in the number of electrons and positive ions; i.e., an avalanche. The electrons sweep quickly toward the anode and the cluster of positive ions moves somewhat more slowly towards the cathode. When the positive ion cluster reaches a critical density, it strongly attracts the electrons so that a large number of recombination events occur and photons of light are generated to such a degree that the cluster of positive ions is brightly luminous and travels at speeds of $\sim 10^7 - 10^4$ cm/sec. Both positive and negative streamers move between the electrodes so that, if visually observed, one could see a group of discrete balls of light, "light globules" or "light pulses" moving in various directions.

In air at high field strengths, the normal color of the streamers is a bright blue since the most frequently excited radiation is from the second positive group of highly excited N_2 molecules. One finds ultraviolet radiation produced in abundance also. In air at low electric fields, the ionization and excitation favor the arc spectrum of N_2 and Nitric Oxide yielding a reddish purple glow. Yellow flashes have sometimes been observed in the streamer corona and this is thought to be due to the presence of Na from NaCl on the electrode surface. In addition, it is thought that if minute carbon flakes are ejected from the electrodes and rendered incandescent in the corona bursts, these could give rise to red or yellow streaks of light. However, a bluish-white color is the overwhelmingly dominant feature of the discharge.

The work of Loeb[5] also discusses observations that allow us to consider the color aspect from a new point of view. Studies are described wherein a sheet of color film is exposed to streamers via (a) the emulsion side and (b) via the non-emulsion side. In (a) the discharge patterns were found to be blue whereas in (b) they were red; i.e., the blue light, entering via the

back side of the film, leads to a red imprint. To fully understand this effect and to see its possible relationship to Kirlian photography, we must consider the layer construction of typical color film (see Fig. 12).

The color film consists essentially of three emulsion layers separated by two filter layers and a transparent plastic backing[4]. When white light impinges on the film from the emulsion side, the U.V. and blue components expose the first layer while the green and red are passed. Only the red and green components pass through the first filter layer and only the red passes through the second filter layer to expose the third emulsion layer. The middle emulsion is an orthochromatic emulsion which is sensitive to green, blue and U.V. and the third emulsion is a panchromatic emulsion sensitive to red, green, blue and U.V. Any attenuation of the red and green components due to passage through emulsion and filter layers is probably compensated for by making the second and third emulsions correspondingly more sensitive.

When white light impinges on the film from the support side, the situation is quite different. In this case, the third emulsion (red) is exposed by all components, the second emulsion (green) is exposed only by blue and the first emulsion (blue) remains unexposed (see Fig. 12). The resulting exposure would be a color mixture of red and green which yields yellow for equal exposure intensities. However, it is to be expected that the red layer will receive a much greater exposure than the green layer yielding an overall result of orange or reddish orange. This effect is enhanced even further by the differing sensitivity of the two layers which have been adjusted to deal with light impinging on the film from the emulsion side. A very similar situation exists when only blue and U.V. light impinges on the film from the support side. However, because of the absence of a red component in the incident light, the composite color

effect will be more towards the orange than towards the red as in the general case of incident white light.

Let us now consider the effect of different spacings between the film and the adjacent electrodes. Imagine that we have placed a film, emulsion side up, in the electrode device and have located it with the emulsion surface at distance d_1 from the upper electrode and the film support surface at distance d_2 from the lower electrode. Let both electrodes be of the same material. If $d_1 \approx d_2 \neq 0$, both positive and negative streamers bombard both sides of the film and, for only blue light generated by the streamers, color film will show both red and blue patterns. If $d_2 = 0$, $d_1 \neq 0$, so that the film is firmly placed against the lower electrode, no streamers can develop on the support side of the film and the color film will show only blue patterns. Conversely, if $d_1 = 0$, $d_2 \neq 0$, so that the emulsion is firmly placed against the upper electrode, no streamers can develop on the emulsion side of the film so the color film will show only reddish orange patterns.

Since we are always using small electrode spacings ($d_1 + d_2 \sim 200\ \mu$), unless very great care is exercised, undulations in the film occur so that d_1 and d_2 vary over the surface of the film resulting in some regions where the exposure is predominantly blue, somewhere it is predominantly reddish-orange, and some of an intermediate hue. This is illustrated in Fig. 13. Our results, indicating blank patches amongst the dots when using film but none when using plates, supports the film distortion hypothesis. The fact that people using polaroid never see anything except blue and white also supports the hypothesis because polaroid film has a fairly opaque backing. Finally, our initial experiments with a transparent electrode have revealed only blue and white patterns of color (no red, yellow or green).

E. The Streamer Model of Electrical Discharge

1. Basic Features

We shall begin by first describing the simplest outlines of the model and then shall elaborate on various subtle aspects during further iterations[5,6].

One may begin by considering a plane-parallel gap of spacing, d = 1 cm, in which the cathode is illuminated by ultraviolet light to such an extent that one electron per microsecond leaves one square centimeter of cathode area. Assume that the atmosphere is air at 1 atmosphere pressure and that the potential between the plates is 31,600 volts (the conventionally observed sparking potential, V_s). The ratio E/p = 41.6 volts/cm per mm Hg, where E is field strength and p is pressure, is an important parameter of the process. A single electron starts across the gap, quickly acquiring an average random energy of $\varepsilon = \frac{1}{2} m v^2 = 3.6$ electron volts and a drift velocity v in the field direction of about $1.5 - 2 \times 10^7$ cm/sec. As this electron moves, it creates new electrons by collision at the rate of α per cm in the field direction (α depends strongly upon E/p) so that, in a distance x, it and its progeny amount to $e^{\alpha x}$ electrons, forming what is called an <u>electron avalanche</u>. Therefore, $e^{\alpha x}$ positive ions have been left behind by the electron group, virtually where they were formed in the 10^{-7} sec during which the electrons traveled between the plates. The mobility of the positive ions is 10^{-2} to 10^{-3} times that of the electrons.

As the electron avalanche advances, its tip is spreading laterally by the random diffusive movement of the electrons. The radial distance of diffusion is readily calculated to be $\bar{r} \approx \sqrt{2Dt}$, where t = x/v is the time of advance of the avalanche, and D is the electron diffusion coefficient

(readily computed from v). From these data, it is possible to compute the density of positive-ion space charge left behind at any point x. The value of α under these conditions is about 17, making $e^{\alpha d} = 2.4 \times 10^7$. The first ion pair is created at 0.04 cm from the cathode and there are 4.9×10^3 ions at 0.5 cm from the cathode, 3.66×10^5 ions at 0.75 cm and, within 0.04 cm from the anode, there are 1.2×10^7 ions. A schematic diagram illustrating this process is given in Fig. 14. Cloud track pictures of such avalanches as they proceed across the gap with time intervals of 10^{-7} sec are shown in Fig. 15.

Most of the electrons will be drawn to the anode except for some few that are bound by the positive ions. Such a distribution of ions does not make a conducting filament of charges across the gap and hence, in itself, an avalanche that has crossed does not constitute a breakdown of the gap. To estimate the number of electrons bound by the positive ions, we need to compute the electric field due to the positive ions. For simplicity, we shall think of the ions as being in a sphere of radius r so that the field strength E_1 due to this space charge is $4/3\ \pi\ r\ e\ N$, where e is the electronic charge, and N is the density of ions. In a distance dx at the end of the path x, the number of ions resulting from cumulative ionization is $\alpha\ e^{\alpha x}\ dx$ and $N = \alpha\ e^{\alpha x}/\pi\ r^2$ so that $E_1 = \frac{4}{3} e\ \alpha\ e^{\alpha x}/r$. Choosing $r = \bar{r}$ caused by electron diffusion in crossing the gap ($\bar{r} = 0.013$ cm by observation), this yields $E_1 = 6000$ volts/cm or $E_1/E = 0.20$. Thus, the field caused by the positive space charge is 20 percent of the applied field near the cathode. If the initial voltage had been increased by 5%, E/p would have been 5% higher (E/p = 43.6) and α would have been 20, which gives $E_1 = 140{,}000$. Thus, for this case, part of the electron swarm would have been held back by the heavy space charge some 0.9 of the way

across the gap unless there are other important factors which we have neglected.

The single most important fact neglected thus far is that a number of secondary mechanisms exist for the formation of electrons in the air gap. Since α is a constant for a given value of E/p, electrical breakdown can occur only if, before disappearing, this first avalanche itself gives rise to a second avalanche at least as dense, and so on. This can happen only as a result of other processes for the production of free charges. Some of these are known and others can be imagined:

(1) β effects: ionization of the gas by collisions with positive ions created by the initial electrons.

(2) γ effect: emission of secondary electrons by the cathode under impact from ions in the discharge. It is this process which explains breakdown at medium pressures. It depends on the nature of the gas and the cathode and can occur only after a considerable delay.

(3) δ effect: emission of secondary electrons by the cathode under impact from photons coming from the discharge (deexcitation or recombination). Since the photons are very fast and scarcely absorbed, this process is very fast and efficient (particularly at high pressures); it depends on the gas and the cathode.

(4) ε effect: emission of secondary electrons by the cathode under impact from excited atoms in a metastable state. The effect is analogous to γ and δ processes but, in this case, the delay is a great deal longer because the atoms diffuse very slowly to the cathode.

(5) η effect: photoionization of the gas. The process can play a significant part at high pressures. In pure gases, it can occur only with great

difficulty since the photons which arise in the gas due to recombination or deexcitation do not have an energy sufficient to ionize the same gas.

For the generation of streamers, it is the η effect that is of prime importance to us. Accompanying the cumulative ionization, there is produced, by the electrons, from 4 to 10 times as many excited atoms and molecules[7]. Some are excited to an energy exceeding the ionizing potential of some of the atoms and molecules present, either by excitation of an inner shell, by ionization and excitation, or in a mixed gas-like air by the excitation of molecules of higher ionizing potential, e.g., N_2 . These atoms or molecules emit radiations of very short wavelength in $\sim 10^{-8}$ seconds. This short ultraviolet radiation is highly absorbed in the gas and leads to ionization of the gas.

The photoelectrons created at points in the gas and at the cathode at any great radial distance from the avalanche axis will merely create more avalanches. Those photoelectrons created near the space charge channel of positive ions, and especially near the anode, will be in an enhanced field which exerts a directive action drawing them into itself.

The electrons from the intense cumulative ionization of such photoelectron avalanches in the combined fields E and E_1 which are drawn into the positive space charge feed into it, making it somewhat of a conducting plasma which starts at the anode. In this fashion, the positive space charge develops toward the cathode from the anode as a self-propagating positive space-charge streamer. The velocity of streamer propagation, dependent as it is on photo-ionization in the gas and photon propagation at the velocity of light as well as the short distance motion of electrons in high fields near the space charge, is rapid. It has been observed to be about 1.3×10^{-8} cm/sec by Roether[5] in one case.

As the streamer advances towards the cathode, it produces a filamentary region of intense space charge distortion along a line parallel to the field. The conducting streamer of a plasma consisting of ions and electrons extending to the anode thus makes a very steep gradient at the cathode end of the streamer tip. As this advances towards the cathode, the photoelectron avalanches produced by radiation at the cathode begin to produce an intense ionization near the cathode. Thus, as the space-charge streamer approaches the cathode, a cathode spot is forming which may become a source of visible light. As the streamer tip reaches the cathode, the high field produces a rush of electrons toward the end of the streamer. This, if followed by a current of electrons, gives a high-potential wave which passes up the preionized conducting channel to the anode, multiplying the electrons present by a large factor. The channel may thus be rendered highly conducting and, unless limited by external resistance, will then develop into an arc. The velocity of propagation of the returning wave of ionization up the preionized channel may be as large as 10^9 to 10^{10} cm/sec in certain instances.

Aside from all the details, the important factor for us to remember is that <u>this is the primary source of light detected in high-voltage photography.</u> It is found that the process does not occur in vacuum, pure, rare or atomic gases, probably because of the absence of any significant photoionization effect. In addition, the process is only possible if the magnitude of E is sufficient for the charge density of the avalanche to reach a critical density N_c [requires $N_c \sim 3 \times 10^8$ ions with $r \approx 3 \times 10^{-3}$ cm arising from $(\alpha d)_c \approx 20$].

As we look a little deeper, we find that all light-emitting streamers do not propagate completely across the interelectrode space but that some are extinguished in midgap. The streamer length depends on the applied voltage, increasing with the voltage. During streamer propagation, some of the initial critical ball of positive ions are consumed by recombination events so that it becomes subcritical and ceases to propagate, i.e., the energy required to create new ion pairs and excited atoms is derived from the energy of the streamer tip.

To investigate the effect of the electrode material on electron emission, the following experiment was carried out at atmospheric pressure: a voltage pulse $V \gtrsim 1.25\ V_c$ was applied to the electrodes for 10^{-2} seconds and the observed current recorded. The number of electrons emitted per second, I, for $E = 10^4$ V/cm is given in the following table. It can be seen that the emission, even at this small field strength, is far from being

Steel			Copper		Nickel	Al-Mg Alloy
Milled	Oxidized	Turned	Drawn	Turned	Turned	Turned
10^6	10^6	5.5×10^3	1.4×10^4	5×10^5	7×10^3	5×10^3

negligible. This experiment also noted a conditioning effect: when the breakdown current is limited to fairly low values, the emission current, I, decreases as the number of tests increase. This would be due to the successive elimination of dust and microscopic irregularities. The study also showed that I varies with E according to the law of cold emission[8] but with

coefficients such that the work function, $\varphi \approx 1$ ev and the effective surface area $S \approx 10^{-14}$ cm^2. These results strongly suggest the mechanism of very localized field emission (perhaps created by chemical contamination or by sharply curved protuberances). In general, we must anticipate a strong geometrical effect due to the field enhancement at any sharply curved point.

The effect of a contaminant for the fossilization of streamers has been illustrated recently by Murr[9]. While studying silicon nitride (Si_3N_4) ribbons in an electron microscope, he found that hydrocarbon contaminant ions polymerized on the negatively charged streamer regions to build up the fossilized corona pictures shown in Fig. 16.

Although the onset of breakdown may depend on the electrode material, the streamer length is not similarly affected. The streamer length is found to be proportional to the applied voltage only. If a photographic film is placed in the point-to-plane gap (see Fig. 17), either perpendicular to and a short distance from the anode point, or parallel to and in contact with the anode point, the streamers move along the surface of the film and leave a photographic record of their path (Lichtenberg figures)[5]. In these experiments, the film seems to act largely as a deflector for the streamer such that the path length in air plus the length along the surface of the film is a constant for constant applied voltage[7].

2. Electrode Polarity Effect

A representative experimental arrangement used for studying streamer characteristics is that of Nasser[10] given in Fig. 17. The point-to-plane electrode configuration is a favored one by corona discharge researchers because it provides a uniform electric field in the vicinity of the plane

electrode and a radially symmetric field in the vicinity of the point electrode having an enhanced field strength due to the reduced radius. Significantly different morphology and features of the discharge exist depending upon whether the point electrode is positive or negative.

The polarity effects recorded with a point-plane or cylindrical electrode arrangement (in Fig. 18) are the result of the different roles played by the electrons and positive ions in the discharge gap. The electrons are fast, ionize in avalanche fashion, and tend to move rapidly to the anode$^{(+ve)}$; the ions are slow, stay behind as positive space-charge clouds and tend to drift toward the cathode$^{(-ve)}$. The original electrostatic field between the electrodes is therefore greatly altered as events unfold.

When the point electrode is positive, the electrons are accelerated into a field of increasing intensity and leave behind radial channels of positive space charge, increasing steeply in charge density toward the anode. This extends the electrical character of the anode, giving it a tenacle-like character which attracts subsequent electrons. As new avalanches strike the radial channels from various directions, a system of positive space-charge branches grows from the positive point electrode into space until, at the tips, the field becomes too weak to support further ionization.

In contrast, from a negative point electrode, the electrons speed out into fields of decreasing strength. Ionizing, they leave behind a positive charge that further weakens the radial driving field and creates tangential field components. Thus, the negative primary discharge broadens into sectors and steepens the field directly in front of the cathode. This tendency causes the primary negative Lichtenberg figure to be smaller than the positive Lichtenberg figure.

A space-charge branch of the positive figure (Fig. 19) may transform into a plasma when a succession of electrons transverse the same path. As the resistance of the branch decreases, more current concentrates in it and its field towards the outside increases. Thus, a positive spark develops as if a metal wire were pushed from the anode along a tortuous path predrawn by the primary figure. Side branches, robbed of their field by the advancing channel, die off. Since the voltage drop along the spark channel is quite small, a positive spark carries the anode potential practically on its tip. New starting electrons are created by the photoeffect in the gas ahead of it. The advance continues, if overvoltage is avoided, by the creation of positive space-charge branches and the transformation of a selected few of these branches into plasma channels. Because the electron flow is a converging flow, the electron density reaches sufficient proportions that the magnetic pinch effect (Lorentz force) becomes operative which squeezes the plasma into narrow channels.

On the other hand, the negative spark can draw on a much more copious electron source provided at the cathode by thermionic or field emissions. The build-up of positive ions at the cathode surface enhances the magnitude of the electric field at the cathode and pulls more electrons out of the cathode. The developing plasma, however, does not find a narrow space-charge branch for intricate guidance but rather a broad sector of space charge and moves forward along a straight smooth path. Cutting radially through the primary figure, the spark may be brought to a temporary halt at its edge if overvoltage is avoided (the electrons are moving into a region of reduced field). Then the advance continues in the direction of the highest space-charge field gradient, which frequently lies tangentially to the old direction. It transverses its path in a number of discrete steps[11]. In

this manner, the most intricate secondary Lichtenberg figures can be created (Figs. 20, 21). Still, the negative spark consists of smooth sections while the positive spark, in its unruly advance, reveals the guiding space-charge tracks.

In Fig. 22, Nasser[12] has shown autographs of ionization obtained at different locations from the negative point. His investigations were conducted using a single voltage pulse having a short rise time of about 1 μsec and a slow decline of the order of a few milliseconds. Applying pulses rather than dc voltages ensured that the film carried no space charge prior to the arrival of the first ionization event. Later processes are modified by the charge present on the film surface. Using long-duration pulses reduced the effect of the reversal of polarity that would have occurred with rectangular pulses in which the voltage, after a duration of a few microseconds, is reduced to zero. This results in the creation of "reversed" high fields between the negative space charge and the point electrode which is now at ground potential. This field gives rise to the function of "backfires" (erratic positive streamers) between the space charges and the point electrodes. Certain features of this study are similar to that of Milner and Smart[13].

With the point positive and facing the sensitive side of the film, the four autographs of Fig. 23 are typical of what is obtained as the film is moved from the point toward the plane. The autograph of Fig. 23(a) was taken with the film almost touching the point, yielding the typical positive figure. Such a figure is produced by a streamer emerging from the point and then deflected by the film. Because of the symmetry of the experimental apparatus, the streamer divides into six branches equally distributed around the circumference of the main branch. The six branches continue to branch further resulting in the pattern shown.

Moving the film 1 cm away from the point resulted in the autograph of Fig. 23(b). Here there are a number of streamer branches, called impact points, out of which surface streamers, similar to those of Fig. 23(a) but having different lengths, grow radially outward. Such an autograph is produced by the several branches developed in the main streamer that strike the film and are then deflected into the field. A single streamer starting at a point may branch into as many as 40 branches. Figure 23(c), taken 1.5 cm away from the point, shows that the number of impact points reaching the film has increased tremendously. The surface tracks (glide streamers) they produce have diminished in length however. From this fact, the electrical potential of streamer tips can be estimated. Finally, Fig. 23(d), taken 2 cm from the point, indicates the enormous number of branches present; most of them have short surface streamers that repel each other. All four autographs were taken with a 30 kV voltage pulse that was well above corona onset but below spark threshold (36 kV). At reduced voltages, the manifestations shown by the autographs become continually less pronounced, finally disappearing.

If very intensive streamers strike the cathode, electron emission is produced. This is due to the high electric field in front of the space charge of the streamer tips approaching the cathode; the emitted electrons are accelerated toward the positive wavefront. If there is ample time and distance, the electrons initiate avalanches and negative streamers. When the current is observed, a pulse is produced when the streamers reach the cathode. A flash of light was also reported when the phenomenon was viewed with the aid of sensitive photomultipliers. A film was placed on the cathode and, depending on the orientation of the emulsion side, either the ionizing processes at the cathode or those emanating from the anode, or both, were recorded. The use of

color film shows both phenomena, with radiation coming through the back side exciting the red-layer emulsion and that coming from the front exciting the blue layer. Streamer impact points and tracks are seen in red, whereas cathode phenomena are seen in blue or white because of their high intensity (see Fig. 24).

3. Back Figures and Retrograde Streamers

On the negative plates taken at low pressures (see Fig. 18), a ghost-like structure generally appears behind the sectors. Increase of pressure sharpens the structure of these "back figures"; they change from broad foggy trees to sparks travelling preferentially along the outer edges of the negative primary discharge figures (see Figure 25). These sparks of pronounced positive character are soon a dominating factor in the landscape of the surface discharge (Figure 26). They follow the negative sparks and climb like ivy over the negative tree trunks (Figure 27). All the evidence indicates that the back figures are lightning strokes discharging the negative clouds when the transient voltage applied across the electrodes die away. Figure 28 schematically describes the situation in terms of surface charge and its removal for a typical case such as Figure 26. After a rapid building up of the positive charge (cathode fall) by the primary negative figure, a negative spark develops from a preferential point, branches sharply and covers an appreciable area with a new primary figure. The external voltage starts to fall and soon the electrode becomes positive with respect to the negative parts of the cloud. At the point of highest gradient, the return flow of electrons starts with sufficiently intense ionization to create a positive spark. Using the large electron supply available in the negative surface charge, the spark grows rapidly and neutralizes the two-dimensional cloud as far as the intensity

of the field allows. The final neutralization of the remaining charge is a slow process of local recombination and conduction without the formation of new traces.

When the feather discharge of Fig. 29 approaches the anode, positive retrograde streamers start to propagate from the positive plane toward the oncoming feathers. This has been detected by axial photographs and is illustrated in Fig. 30. The lateral extent of the anode action was revealed by placing a film on or near the plane with the photographic emulsion facing the plane. The retrograde streamers emerging from the anode cannot proceed towards the opposite electrode. Instead they strike the film producing patterns similar but not identical to those obtained at a positive point[10] (see Fig. 31). The pattern revealed can take a number of forms that depend on the cross section, number and distribution of the oncoming feathers. If the envelope enclosing the feathers is circular, a circular pattern enclosing the positive streamers is obtained as in Fig. 31. If the envelope is irregular, its exact image is reproduced on the anode since this is the area where high fields are created by oncoming feathers (see Fig. 32).

4. Effect of Electronegative Gases

The influence of electronegative gases on the discharge is helpful for establishing the role played by the positive space charge. Addition of carbon-tetrachloride vapor to nitrogen changes the structure of the primary discharge figures completely. Not only does the diameter shrink to a small fraction of its initial size but also the fine structure of the positive branches and the sharp division of the negative sectors is lost (Figure 33). This decisive activity of small admixtures of carbon tetrachloride is easily understood. Electron impact splits the carbon-tetrachloride molecules into

two highly electro-negative components, CCl_3 and Cl. Both trap slow electrons, thus hindering the start and quenching the growth of electron avalanches. The negative ions formed drift slowly through the field like the positive ones, smoothing out the boundaries of the positive space charge. No sharp negative sectors appear and, instead of the far-reaching positive branches, only short leaves are formed.

The activity of a suppressor gas (organic vapors are found to be extremely effective) is not constant. The decomposition of the original molecule into electro-negative components, the trapping of electrons by the decomposition products and the release of electrons from negative ions by violent collisions depend on the character of the gas and the experimental conditions. Figures 34 and 35 plus Figs. 20 and 33 illustrate the altered discharge morphology due to the presence of a suppressor gas for both positive and negative points. In Figs. 33(a) and 34, we note the appearance of radial spikes of enhanced ionization. In the case of the negative figure, Merrill and Von Hippel[11] assume that the negative space charge may become so dense that electrons at the outer boundary are projected outwards starting new avalanches. In some cases periodic ring structures are formed by periodically revived ionization. These effects disappear if the electro-negative gas is highly concentrated.

The initial breakdown condition is found to be very dependent on the surface condition of the electrodes. Roughening of one electrode, whether it is positive or negative, reduces the breakdown voltage by approximately the same amount. Self-sustaining discharge currents exist before breakdown, decreasing in magnitude with increasing smoothness of the electrode surfaces. Both observations indicate the importance of point discharge

created at rough spots on the surface for the final breakdown. Figure 35 dramatically shows how, at preferential points, the primary figure changes into a spark discharge and, out of this plasma stem, electron clouds are erupted into space.

The effects of enhanced oxygen content in the air plus the effect of humidity on point-to-plane electrode discharges are shown in Figs. 36 and 37, respectively.

F. Electrode Polarization Effects

In the last section, a number of results were shown from conventional streamer studies that strongly parallel Kirlian photography studies[14]. To complete the picture we must consider the induced electric field in the object under study which arises as a result of the driving field of the electrodes.

When an electric field is applied to an electrode system, two important classes of effects occur: (a) geometry effects and (b) time effects. To consider the first, let us consider what happens when a static electric field, E, is applied between an anode and a cathode. Let us initially assume that they are both smooth parallel surfaces. The application of the field E may produce three effects. (i) The emission of electrons from the cathode which may accelerate and produce a sheath of positive ions at the cathode leading to an enhanced field immediately adjacent to the cathode and a decrease in the region beyond. This is called the cathode fall (see Fig. 38). (ii) The induction of an additional dipole moment at the surface of electrodes due to polarization forces. This applies particularly to a leaf or to a surface of skin in the applied field. A dipole layer of opposite sign to the applied field is created at the surface and this generates an electrical potential

shift on the two sides of the surface (see Fig. 39). (iii) The cathode fall and the dipole layer combine to influence the electron emission from the cathode. The former enhances the emission while the latter retards the emission.

For a curved surface, the point effect develops and the applied field is accentuated at the curved surface (the field enhancement at the surface will be almost inversely proportional to the radius of curvature of the surface). In addition, for a polarizable material, the induced dipoles in the material will produce a field of opposite sign that will now vary with distance from the surface. The magnitude of the effect will be proportional to the difference in dielectric constant between the material being studied and air. For example, if we consider a spherical dielectric placed in a uniform field as illustrated in Fig. 40(a), the applied field will induce an electrical dipole in the material which can be thought to be located at the center of the sphere. The field strength associated with this dipole will fall off with the cube of the radial distance from the center of the sphere[3]. Thus, the effective field which is the sum of (a) the applied field, E_a, (b) the shape field, E_s, and (c) the induced field, E_i, will no longer be uniform but may be significantly altered so that streamer formation and the attendant light emission will also be altered by this polarization effect. For two or more such objects, field-line distortion would be such as to create seeming discontinuities between the objects. When one considers the geometrical variations on the surface of a finger placed adjacent to a film-electrode combination as illustrated in Fig. 40(b), it should be evident that great field distortion will occur in the vicinity of the film and that the array-like shape of the finger surface may give rise to special effects of a diffraction type nature.

Turning now to the time effect, we must anticipate that the effective dielectric constant of the medium will be a complex quantity which depends

on the material properties of both the material being studied and the air gap, the temperature and the frequency of the applied electric field, E_a. Two possibilities exist; in some cases the polarization is in phase with the alternating field; in other cases there is a noticeable phase difference between the two. In the first case, no energy is absorbed by the dielectric from the E.M. field whereas, in the second case, we have a dissipation of energy in the dielectric (which is called dielectric loss). The dissipated energy per cm^2 of the dielectric per second is proportional to sin δ where δ is the phase angle between the applied field and the electric current density, i. This phase difference can be due to four different mechanisms: (a) Electrical conductivity, leading to a component of i in phase with E_a, (b) Relaxation effects in connection with permanent dipoles. At low frequencies, the field changes slowly enough to allow the permanent dipoles to reach the equilibrium distribution in the external field before this field has measurably changed. When the frequency of the field exceeds a certain limit, however, the orientation of the permanent dipoles cannot follow the field without measurable lag. This frequency limit is dependent on the chemical composition, the structure of the material and the temperature. In the case of bulk water at $20^{\circ}C$, for instance, there is no appreciable phase difference when the frequency is smaller than 2×10^{9} sec^{-1} (for confined water in membranes, the frequency will be much smaller). For larger polar molecules, this frequency may be reduced by several orders of magnitude. (c) Resonance effects, due to rotation or vibration of atoms, ions, electrons, cells, glands, etc. These effects are noticed in the infrared, visible and U.V. regions, in the neighborhood of the characteristic frequencies. (d) For heterogeneous systems consisting of one or more dispersed phases in a matrix material, the loss angle, δ, is found to be extremely dependent on both the shape and the nature of the particles.

Biological tissues may be represented electrically by an equivalent network which is shown in its simplest form in Fig. 41. The leaky condenser, which is symbolized by C and R_2, is a function of the polarizability of living tissues due to the properties of the cell membrane. R_1, the internal resistance of the organism, may be measured with a high frequency alternating current when it is found to be small relative to the effective resistance at low frequencies. For practical purposes, therefore, living tissues behave at low frequencies like a condenser and resistance in parallel. During the psychogalvanic reflex, the resistance of the skin drops and this charge can be measured with a direct current. The associated change in impedance depends also upon the behavior of the condenser which is still a subject of dispute. Various estimates of the skin capacitance put it in the region, $C \approx 0.01 - 0.03$ $\mu f/cm^2$ for the skin of the forearm and the hand, and values of R_2 range between 25×10^3 and 10^6 ohms.

In one study[15], the impedance of the human skin was found to decrease from approximately 130×10^3 to 30×10^3 ohms as the frequency of the A.C. input increased from 1 to 1000 cycles per second. Over the same range of frequencies, the phase angle, δ, changed from -2 to -58 degrees. In addition, changing the peak to peak current through the subject from 14 to 62 microamperes had no effect on either the impedance of the skin or the phase angles.

In our model of the skin or a plant surface, we must think in terms of a composite system as illustrated in Fig. 42. The inner layer is a reasonably good ionic conductor. The outer layer is quite thin and is of high resistance except in narrow channels of intermediate conductivity at the location of acupuncture points (and perhaps other points). If we consider recent experiments on thin films of mylar polyethylene and polystyrene to which a high electric field has been applied[16], we find that an oscillatory

discharge occurs at fields in the vicinity of 10^6 volts/cm. The current is ~1 μamp with a period of ~1 sec (depends on temperature). Similar current oscillations occur in germanium[17] and other semiconductors at some critical current (critical field). This effect is probably due to a "streamer" type avalanche process in these solids analogous to that which occurs in gases. We can anticipate that this type of phenomenon may occur in the stratum corneum of the skin surface (especially via the acupuncture channels). In addition, a similar process could occur across the photographic film and might expose the different color layers from internal ionization.

To summarize this section, we note the existence of (a) simple geometry (shape) effects which lead to an effect on electron emission, streamer velocity, direction and light intensity; (b) array geometry effects — because of superposition effects of the induced electromagnetic fields (acts like an antenna array) one might expect special spiking and diffraction effects at certain locations and certain frequencies; (c) simple phase angle effects which lead to a phase angle between the driving field and the induced surface field that depends upon driving frequency; (d) heterogeneous surface phase angle effects — at acupuncture points or other points versus normal skin, the phase angle will be different so that the δ-field will have a geometrical character, too; (e) other time variation effects — because of carrier trapping in the skin due to current flow through the skin and to normal decay procedure, the surface potential and skin conductivity will vary with time (and position) so that δ will be a function of both position and time. We can thus expect to see certain resonant frequency effects and certain twinkling effects associated with moving emission patterns.

G. Where Do We Go From Here

To move forward and reliably identify psychoenergetic effects via high voltage photography, we must monitor those parameters of the system that can directly influence the "streamer" process. These are fivefold:

(1) A change in the electrostatic potential, ϕ, of the skin leads to a change in the half-cycle voltage difference between the skin and the driving electrode. Such a change in voltage affects the maximum possible streamer length which determines the width of the corona around a finger tip, for example. Since we know that emotional changes in the human organism can increase the skin potential by up to 500 percent, this effect should be noticed in the corona width and corona brightness.

(2) As a result of mental or emotional state changes in the organism, one may expect to find a change in the surface chemistry of the skin. This effect should give rise to electronegative ion type effects which would alter the morphological character of the discharge. In addition, weak color radiations may come from the excitation of these molecules. It should be noted that small electrical arcs can create hot spots on an electrode as much as 2000°C higher than the ambient temperature; thus, we should not be too surprised if the corona discharge produces a sufficient hot spot to evaporate and ionize organic molecules from biological specimens.

(3) The geometrical induced field effect due both to shape and polarization of the skin surface will lead to certain types of diffraction effects resulting from the spatial and time variation of the dielectric properties of the skin. In order to reproduce and control the "cut-leaf effect" reported by the Soviets[8], this type of wave interference effect will need to be studied very carefully.

(4) As a result of the driving field on the electrode, we should anticipate some type of resonant energy coupling with the cells of the object. This, in turn, may lead to energy emissions from the cells which could influence the ionization properties of the gas and thus alter the quantitative details of the electron avalanche process.

(5) A change in the electrical impedance of the skin or the surface membrane of a plant will serve to alter the "external circuit impedance" of the electrode system. Since it is the external circuit impedance that largely controls the amount of current flow during the corona discharge, both the light intensity and the film buckling effect (for contact photography) will be strongly influenced by the electrical impedance of the biological subject. It is well-known that this varies quite strongly with change of emotional and mental states.

(6) As a final word of caution, we should recognize the fact that such an electrical discharge is a severe perturbation to the energy states of the biological specimen so that one should not pulse the system too severely and should let it relax and recuperate before repeated stimulation.

In conclusion, I believe it is fair to say that we now know what is the physical process for generating Kirlian photographs. We now know that film buckling is the primary reason for the non-blue or white color in high-voltage contact photography but we also know that it is a non-random occurrence. We also know that we have not been sufficiently careful experimentally in the past but we now know what types of biological effects we are looking for. Thus, now, our search can truly begin!

References

1. S. Ostrander and L. Schroeder, "Psychic Discoveries Behind the Iron Curtain" (Prentice Hall, New York, 1970).
2. T. Moss and K. Johnson, Psychic Magazine, July 1972.
3. W. A. Tiller, Proceedings of the Academy of Parapsychology and Medicine's Symposium on The Dimensions of Healing (Stanford University, September 1972).
4. D. Boyer and W. A. Tiller, To Be Published in J. Appl. Phys., 1973.
5. L. B. Loeb, "Electrical Coronas — Their Basic Physical Mechanisms" (University of California Press, Berkeley, 1965).
6. L. B. Loeb and J. M. Meek, "The Mechanism of the Electric Spark" (Stanford University Press, Stanford, California, 1941).
7. G. A. Dawson and W. P. Winn, Z. Physik 183, 159 (1965).
8. W. A. Tiller, "Galaxies of Life," S. Krippner and D. Rubin, eds. (Gordon and Breach, New York, 1973).
9. L. E. Murr, Phil. Mag. 25, 721, 1972.
10. E. Nasser, J. Appl. Phys., 42, 2839, 1971.
11. F. H. Merrill and A. Von Hippel, J. Appl. Phys., 10, 873, 1939.
12. E. Nasser, IEEE Spectrum, November, p. 127, 1968.
13. D. Milner and T. Smart, "There Are More Things," To Be Published.
14. S. Krippner and D. Rubin, "Galaxies of Life" (Gordon and Breach, New York, 1973).
15. R. Plutchik and H. R. Hirsch, Science, 141, 927 (1963).
16. N. Swaroop and P. Predecki, J. Appl. Phys., 42, 863, 1971.
17. W. G. Gurion and D. K. Ferry, J. Appl. Phys., 42, 2502, 1971.

Figure Captions

Figure No.

1 Circular orbits of the hydrogen atom showing the electron in the n = 3 orbit plus possible energy transitions between orbits.

2 Weight on a spring representation of a simple harmonic oscillator of resonant frequency ν_o .

3 Intensity versus frequency plot for a single electron transition.

4 Effect of oscillator coupling on the broadening of frequency. The example used here is that of a gas of varying density, each molecule or atom representing an individual oscillation. At low gas densities (large distances, r) coupling is negligible and all atoms radiate (or absorb) within the same narrow frequency interval. As two atoms are brought closer together, they form a coupled resonant system at two diverging frequencies (black regions). When more atoms are added to the coupled system, additional frequencies appear, favoring the upper region (indicated by the degree of shading). The frequency distribution at the smallest r represents the density of states for a solid or a very dense gas.

5 Intensity versus frequency plot for an idealized physical solid (many atoms interacting).

6 Schematic spectral distribution curve illustrating, along one coordinate, relative radiation characteristics of the seven levels of substance.

7 Energy-velocity relationships for particles between the physical and the etheric frames.

Figure No.

8 Block diagram of high voltage discharge equipment.

9 Schematic of Oudin coil.

10 (a) Photograph of coin (U.S. nickel); multiple pulses, pulse width = 100 μsec, rep rate = 20 Hz, duration = 2 sec. 2X.

(b) Photograph of coin (U.S. nickel); single pulse, pulse width = 100 μsec. 2X.

(c) Photograph of fingertip; multiple pulses, pulse width = 100 μsec, rep rate = 20 Hz, duration = 2 sec. 2X.

(d) Photograph of fingertip; single pulse, pulse width = 100 μsec. 2X.

11 Photographs of single pulse discharge between flat, polished brass electrodes under conditions of different pulse exposure, electrode spacing and orientation. 4X.

(a) Pulse width = 100 μsec

(b) Pulse width = 500 μsec

(c) Pulse width = 500 μsec; nonparallel electrodes, slight increase in electrode spacing.

(d) Pulse width = 500 μsec; electrode areas nonconcentric.

(e) Pulse width = 500 μsec; local film buckling.

(f) Pulse width = 500 μsec; local film buckling for nonconcentric areas.

12 Color film construction, a schematic representation of the effect of U.V. and visible light exposing the film from the emulsion side versus from the support side. Dot in light path indicates exposure of emulsion.

Figure No.

13 Representation of film bending shown in exaggerated scale.

(a) Film bent, electrodes planar, film exposure from left to right will be blue, white (blue, red green) and orange (red, green), respectively.

(b) Equivalent topological configuration to that in (a), except that the electrodes are bent and the film is planar. All intermediate combinations of (a) and (b) are also possible.

14 Schematic illustration of electron avalanche process.

15 Cloud track photograph of streamers from the side.

16 Corona streamer development sequence on silicon nitride crystal.

(a) Streamers just developing on the edges.
(b) After 1 min in beam.
(c) After 3 min.
(d) After 5 min.
(e) After 15 min.
(f) Selected-area electron diffraction pattern in the very end region of (e) showing diffuse, broad ring pattern of carbonous material composing the fossilized corona streamers superimposed on the single-crystal $Si_3 N_4$ spot pattern.

(Courtesy of L. E. Murr).

17 Experimental arrangement for studying streamer development photographically.

18 Positive and negative Lichtenberg figures (positive: 1 atm, 10 kV, point-ring electrode arrangement; negative: 200 mm, 3 kV, point-plate electrode arrangement). (Courtesy of A. von Hippel)

Figure No.

19 Onset of transformation of positive space-charge branches into plasma channels. (Courtesy of A. von Hippel)

20 Intricate negative spark pattern guided by field buildup of the primary discharge (4.5 kV, 1 atm air + CCl_4 saturation pressure) (Courtesy of A. von Hippel)

21 Negative spark developing in steps (1 atm, 10 kV, elliptical electrode). (Courtesy of A. von Hippel)

22 A series of lateral photographs taken at increasing distance from a negative point cathode of 0.05 mm radius, 51 kV and 5 cm electrode spacing.

(a) 0 cm, (b) 1.0 cm, (c) 1.5 cm

(Courtesy of E. Nasser)

23 Autographs from positive point, 30 kV pulse with 2.5 cm interelectrode spacing.

(a) 0 cm, (b) 1.0 cm, (c) 1.5 cm, (d) 2.0 cm.
(Courtesy of E. Nasser)

24 (a) Positive print of negative streamers on the cathode just below spark breakdown, using a single emulsion film facing the cathode.

(b) Negative on a double emulsion film at the same position showing the streamers.
(Courtesy of L. B. Loeb)

25 Negative sparks with primaries and back-figure sparks (11 atm air, 50 kV). (Courtesy of A. von Hippel)

26 Negative primary figure, negative spark and back-figure forming a landscape (16 atm. air, 30 kV). (Courtesy of A. von Hippel)

27 Negative sparks followed by back-figure sparks (18.5 atm. air, 50 kV). (Courtesy of A. von Hippel)

Figure No.

28 Development of the back-figure. (Courtesy of A. von Hippel)

29 Axial autograph at a voltage of 60.4 kV showing the development of a positive retrograde streamer at the right (negative point, 1 atm. air). (Courtesy of E. Nasser).

30 Same as Fig. 29.

31 Lateral autograph with the emulsion facing the positive plane showing the positive streamers developing from it (negative point, 1 atm. air). (Courtesy of E. Nasser).

32 Same as Fig. 31, showing a different random pattern. (Courtesy of E. Nasser).

33 The influence of CCl_4 vapor on size and structure of the primary figures.
(a) Positive figure in 1 atm. N_2 + sat pressure CCl_4, 30 kV.
(b) Negative figure in 227 mm N_2 + sat pressure CCl_4, 3 kV.
(Courtesy of A. von Hippel)

34 Positive primary figure and sparks in Freon (410 mm CCl_2F_2, 3 kV). (Courtesy of A. von Hippel)

35 Electronic eruptions (7 atm. air + saturation pressure CCl_4, 20 kV). (Courtesy of A. von Hippel)

36 Lichtenberg figures at 1, 3, and 4 cm from a 1-mm diameter point in air with an 8-cm gap, and in N_2 with 36 % oxygen, showing the strong suppression in branching and axial range. (Courtesy of L. B. Loeb)

37 Influence of water vapor content on the range and branching of Lichtenberg figures. Upper series for dry air at 2, 3, and 4 cm; lower series for air saturated with water vapor at 22°C at the same distance. (Courtesy of L. B. Loeb)

Figure No.

38 Buildup of cathode fall by positive space charge development.

39 Electrical potential shift resulting from a planar dipole sheet.

40 (a) Distortion of uniform field due to spherical dielectric.

(b) Illustration of geometrical variations on finger surface which influences field.

41 A simple electrical model of skin impedance.

42 Sample physical model of the heterogeneous electrical nature of the skin.

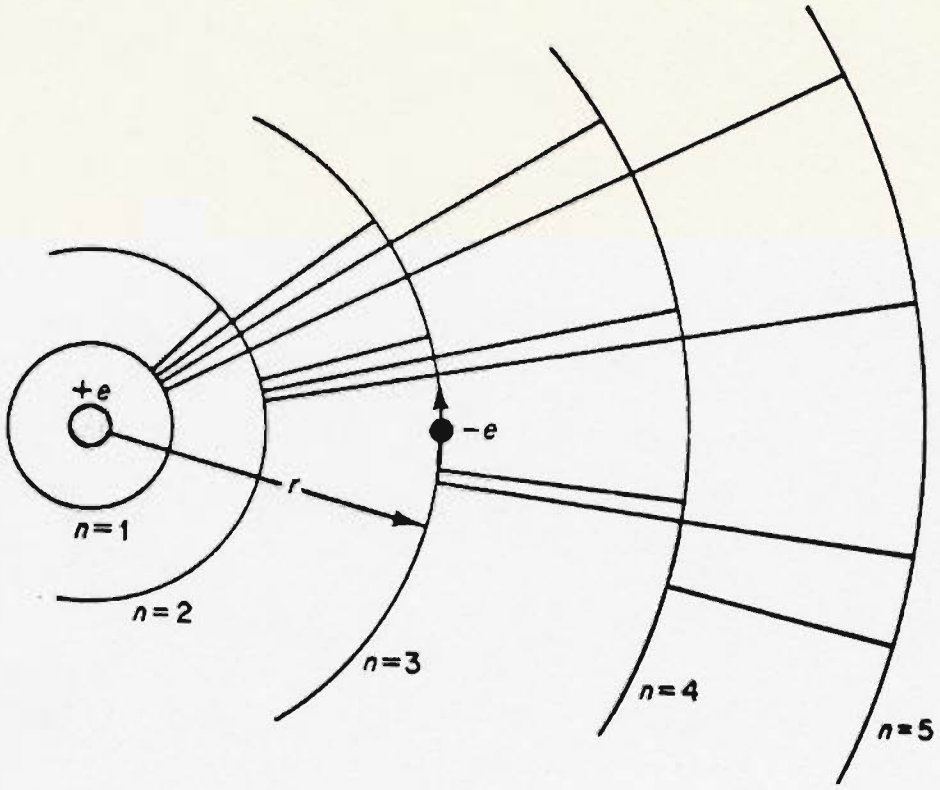

FIGURE 1

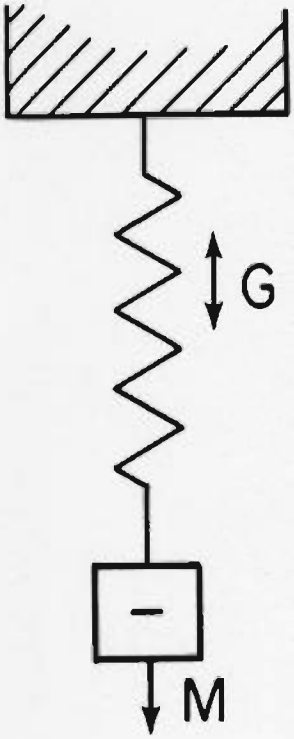

$$\nu_o = \frac{1}{2\pi}\sqrt{\frac{G}{M}}$$

FIGURE 2

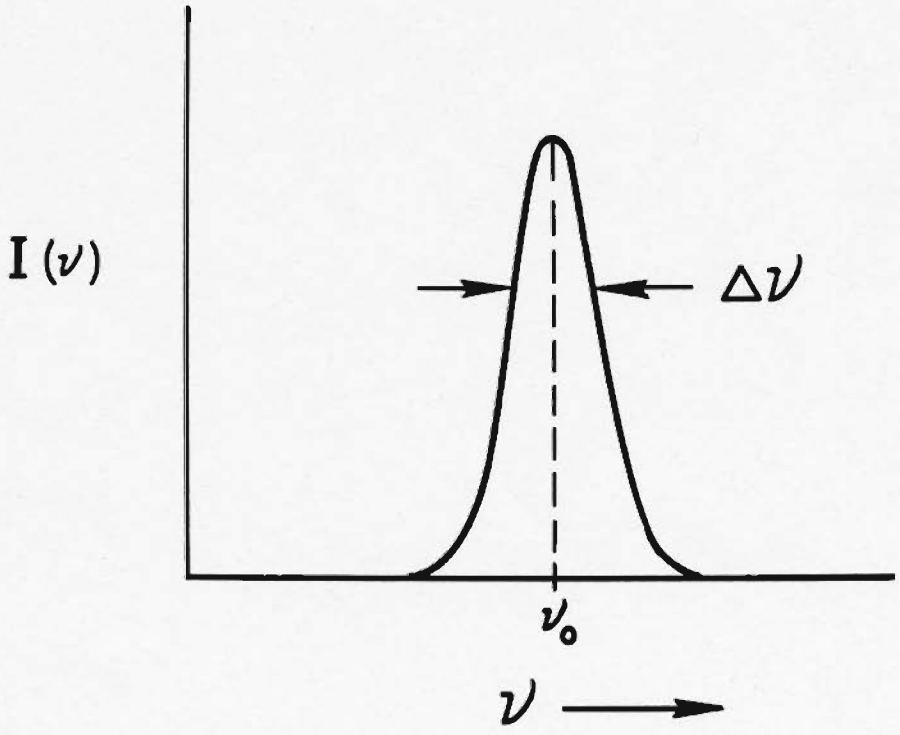

FIGURE 3

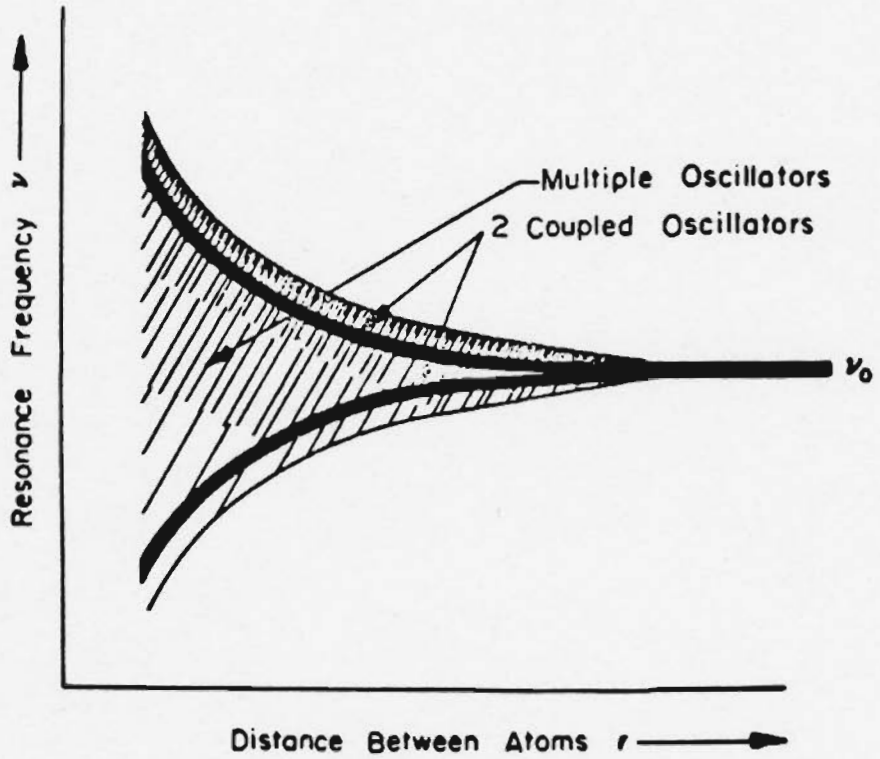

FIGURE 4

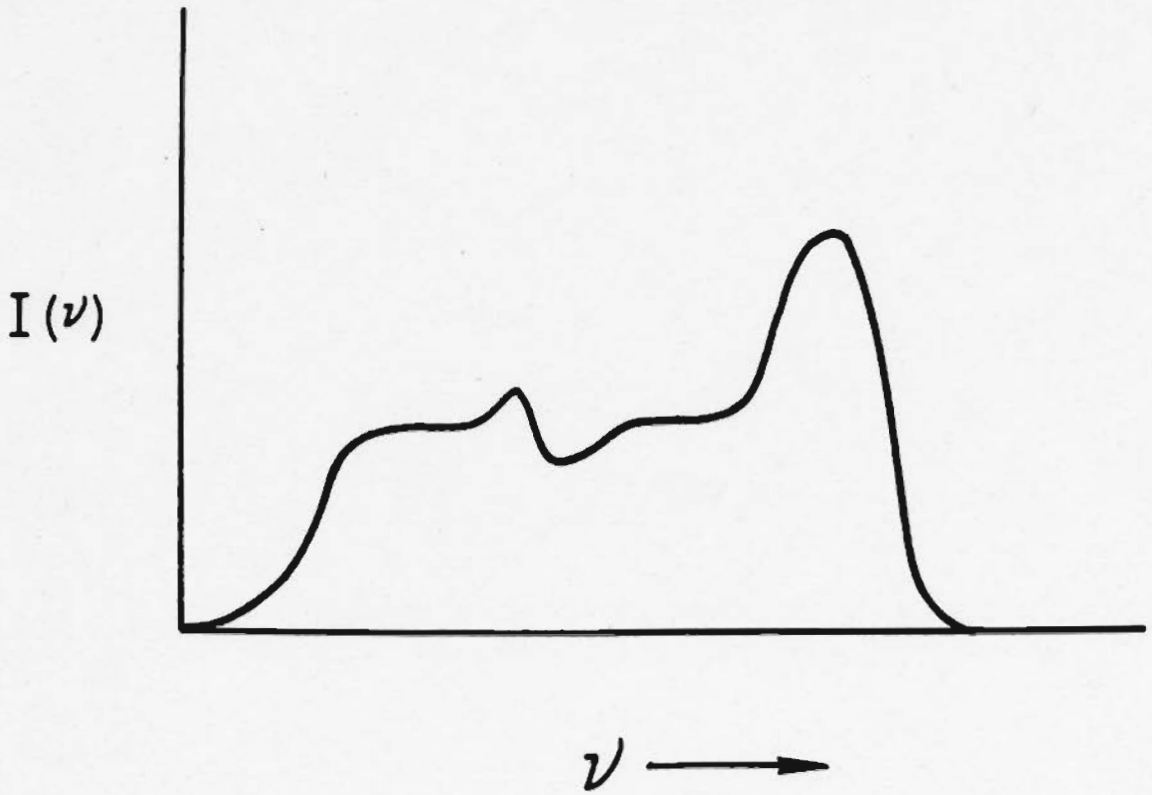

FIGURE 5

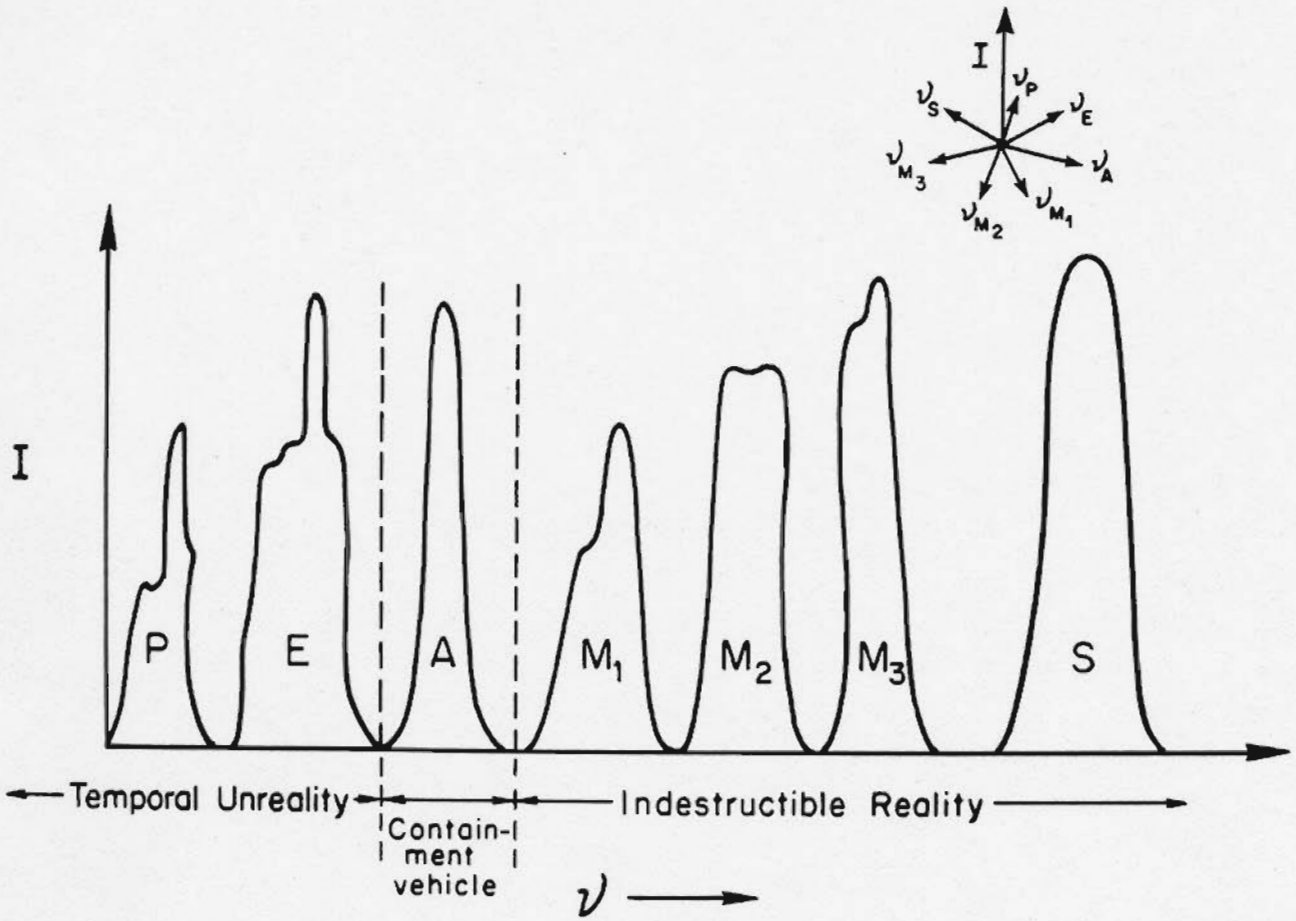

FIGURE 6

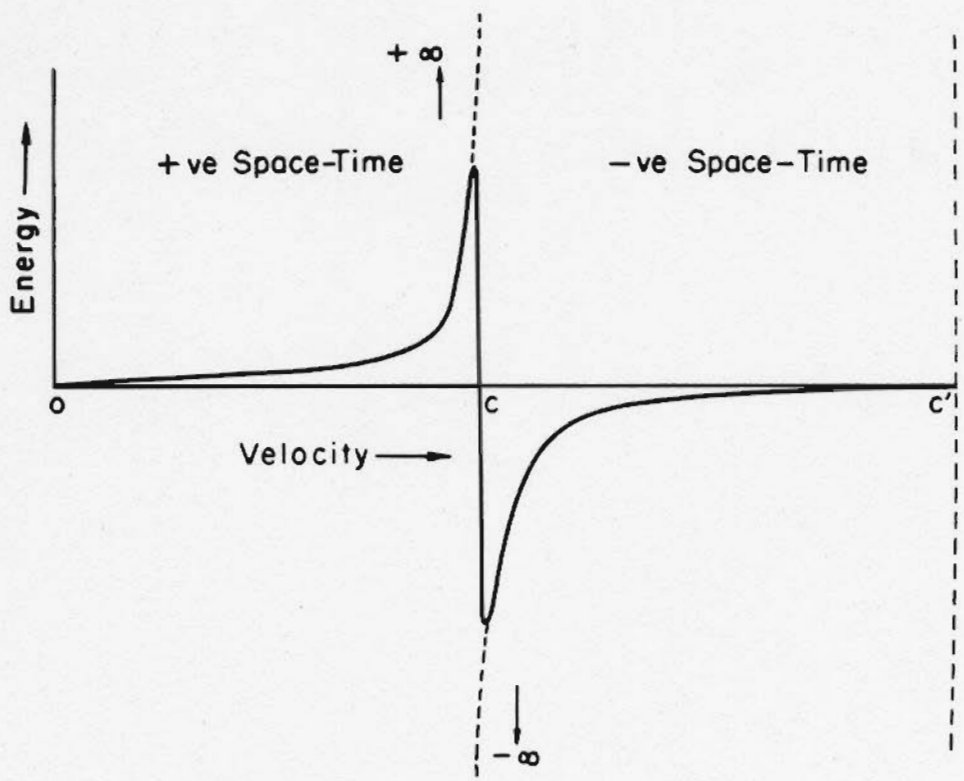

FIGURE 7

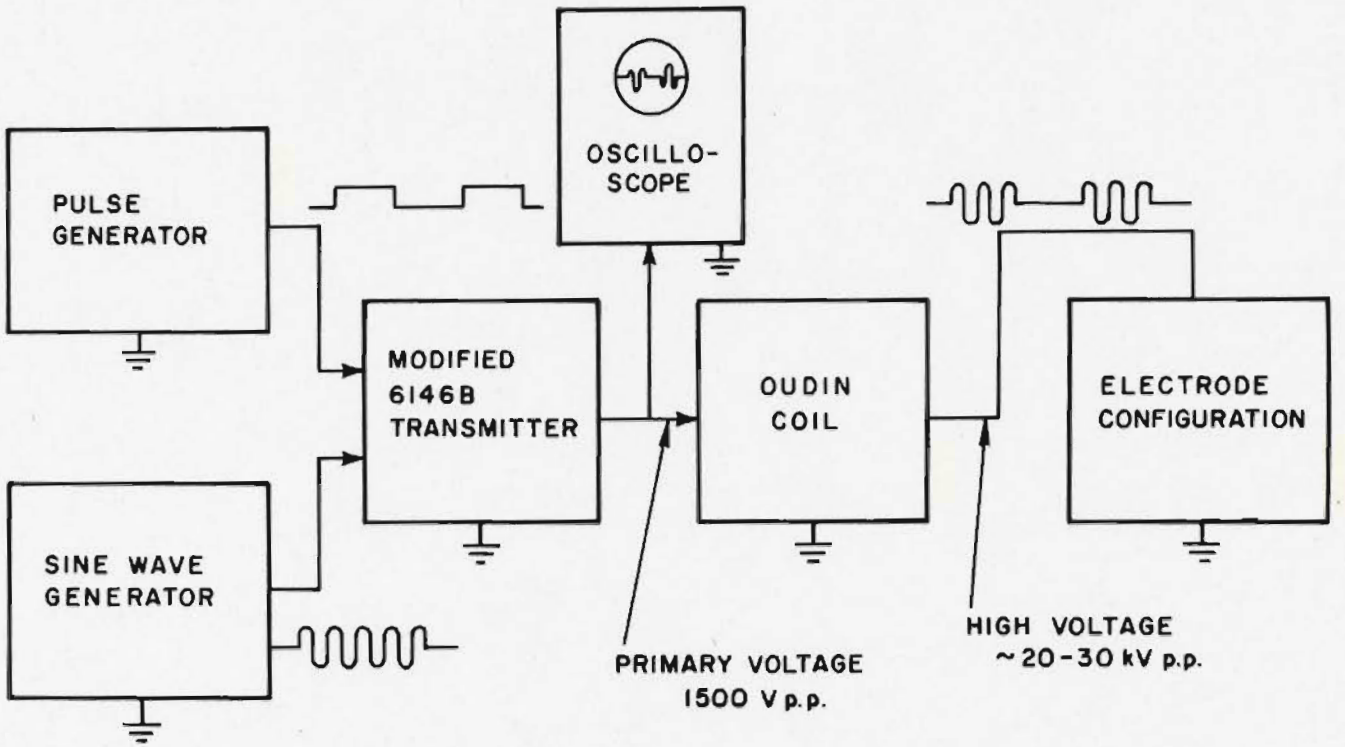
PULSE GENERATOR
OSCILLO-SCOPE
MODIFIED 6146B TRANSMITTER
OUDIN COIL
ELECTRODE CONFIGURATION
SINE WAVE GENERATOR
PRIMARY VOLTAGE 1500 V p.p.
HIGH VOLTAGE ~20-30 kV p.p.

FIGURE 8

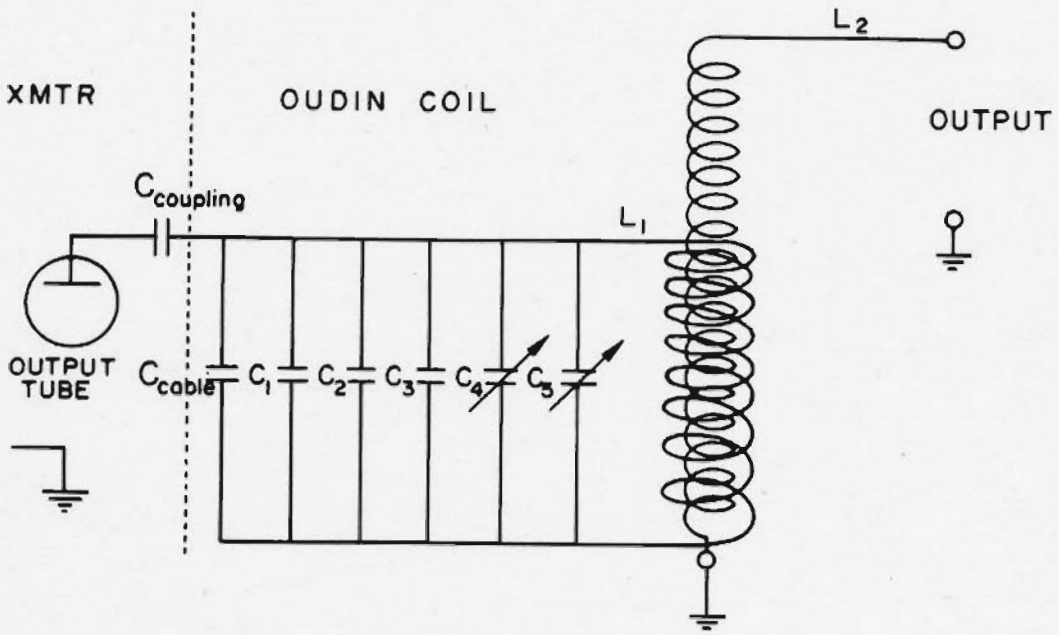

C_C = 100 pf = coaxial cable capacitance

$C_{coupling}$ = 500 pf, 5 kv

C_1 = 500 pf, 5 kv

C_2 = 500 pf, 5 kv

C_3 = 100 pf, 5 kv

C_4 = 23-98 pf, 7 kv

C_5 = 23-98 pf, 7 kv

L_1 = primary coil - 15 turns, 3/16" dia copper tubing, 5" dia, 5" long, supported by lucite supports

L_2 = secondary coil, 500 turns, 24 AWG enameled wire, 3½" dia, 10" long, wound on fiber board tube 12" long.

FIGURE 9

(a)

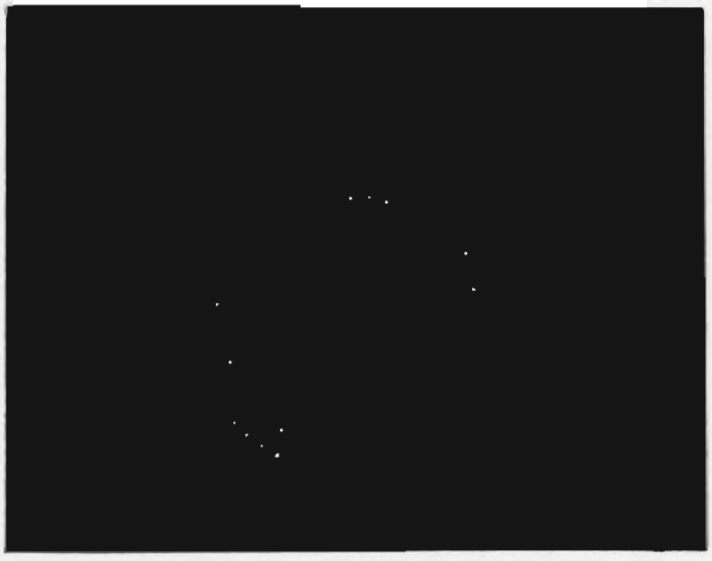

(b)

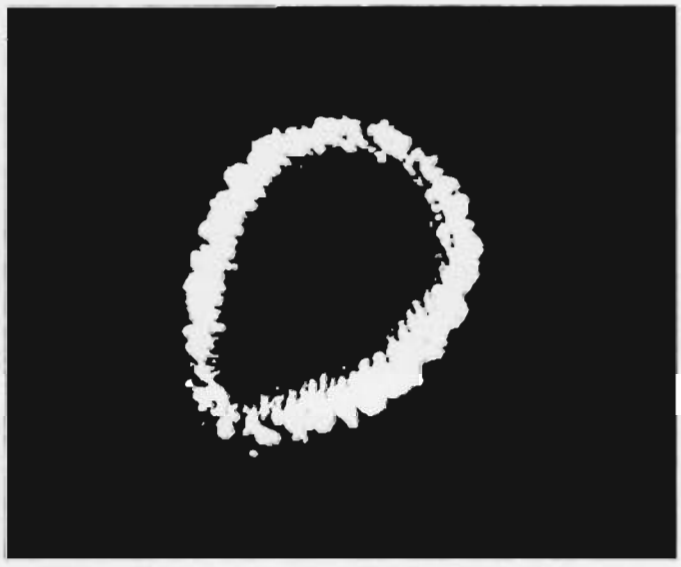

(c)

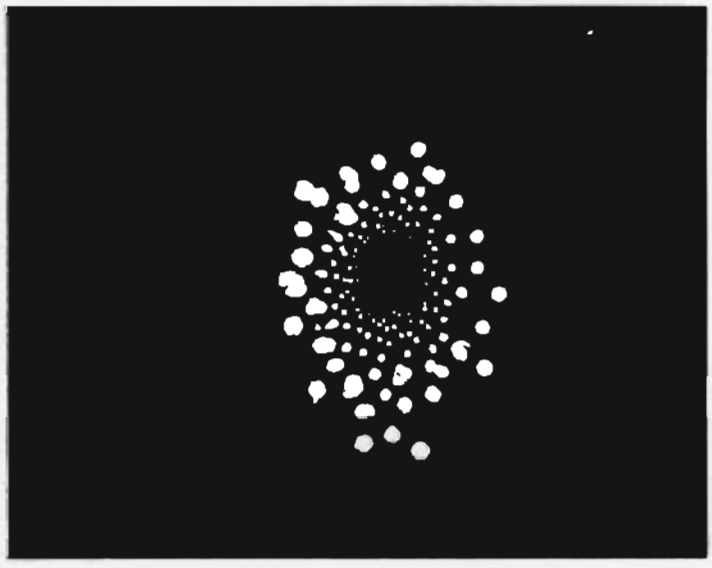

(d)

FIGURE 10

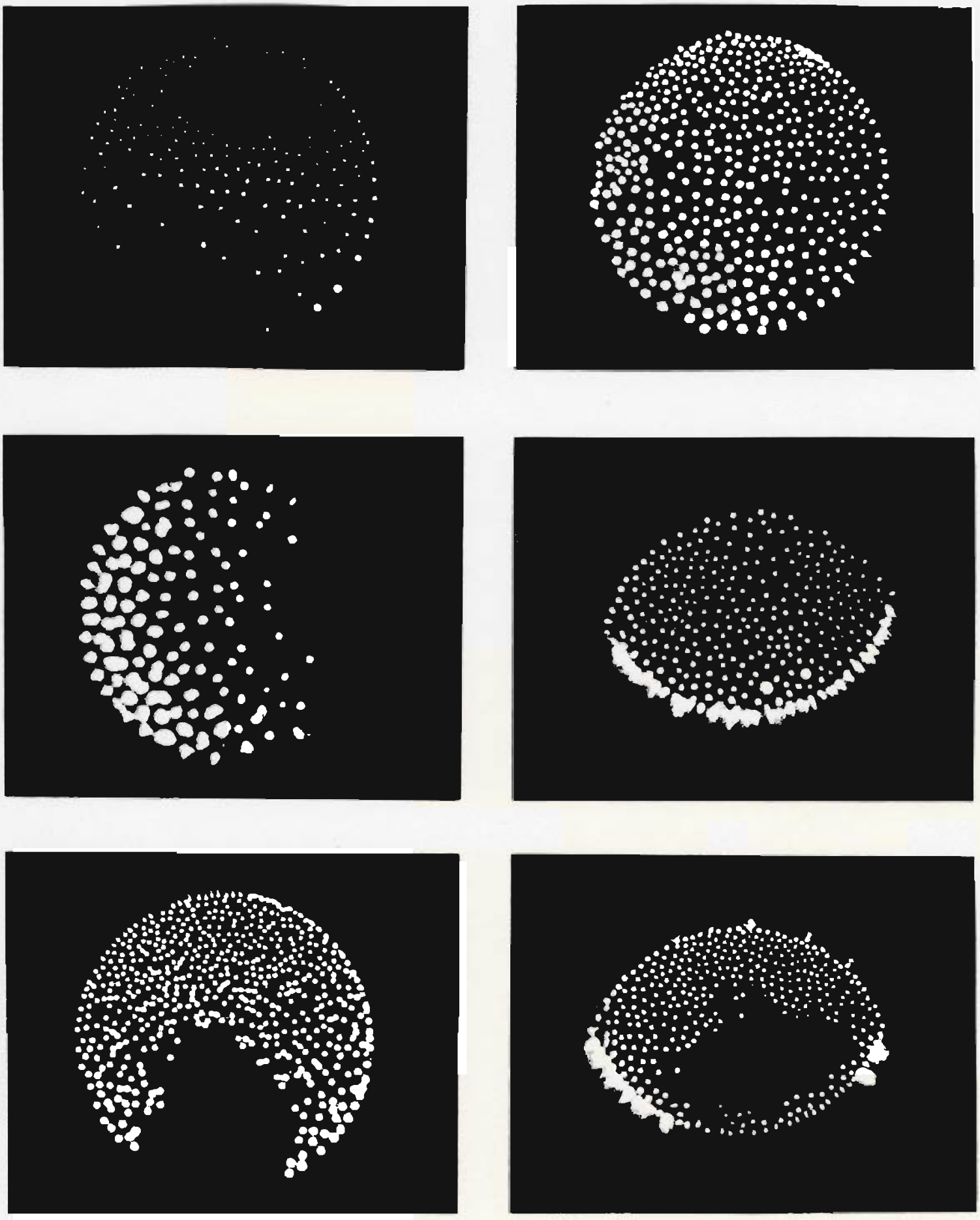

FIGURE 11

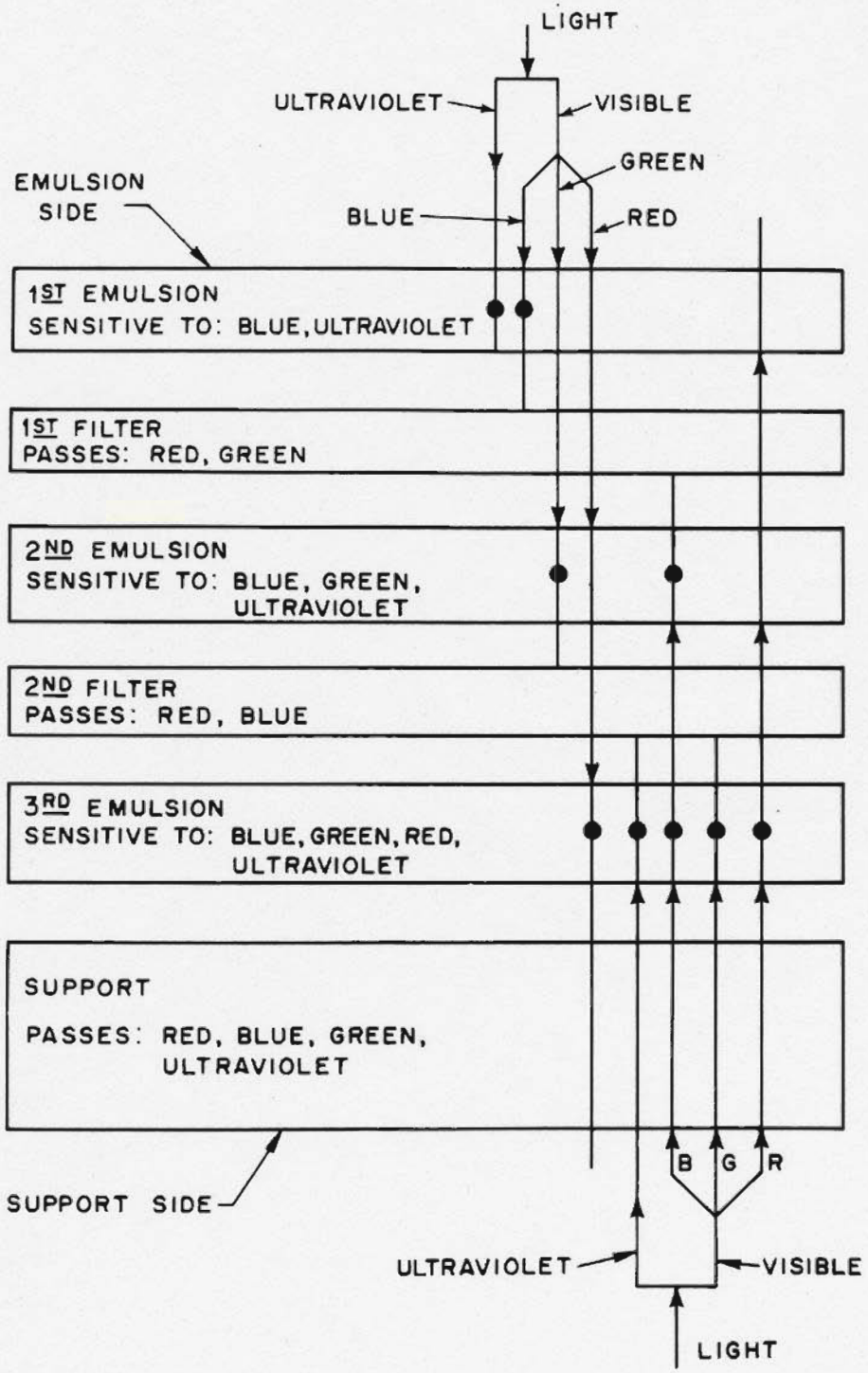
LIGHT
ULTRAVIOLET
VISIBLE
GREEN
EMULSION SIDE
BLUE
RED
1ST EMULSION
SENSITIVE TO: BLUE, ULTRAVIOLET
1ST FILTER
PASSES: RED, GREEN
2ND EMULSION
SENSITIVE TO: BLUE, GREEN, ULTRAVIOLET
2ND FILTER
PASSES: RED, BLUE
3RD EMULSION
SENSITIVE TO: BLUE, GREEN, RED, ULTRAVIOLET
SUPPORT
PASSES: RED, BLUE, GREEN, ULTRAVIOLET
SUPPORT SIDE
B
G
R
ULTRAVIOLET
VISIBLE
LIGHT

FIGURE 12

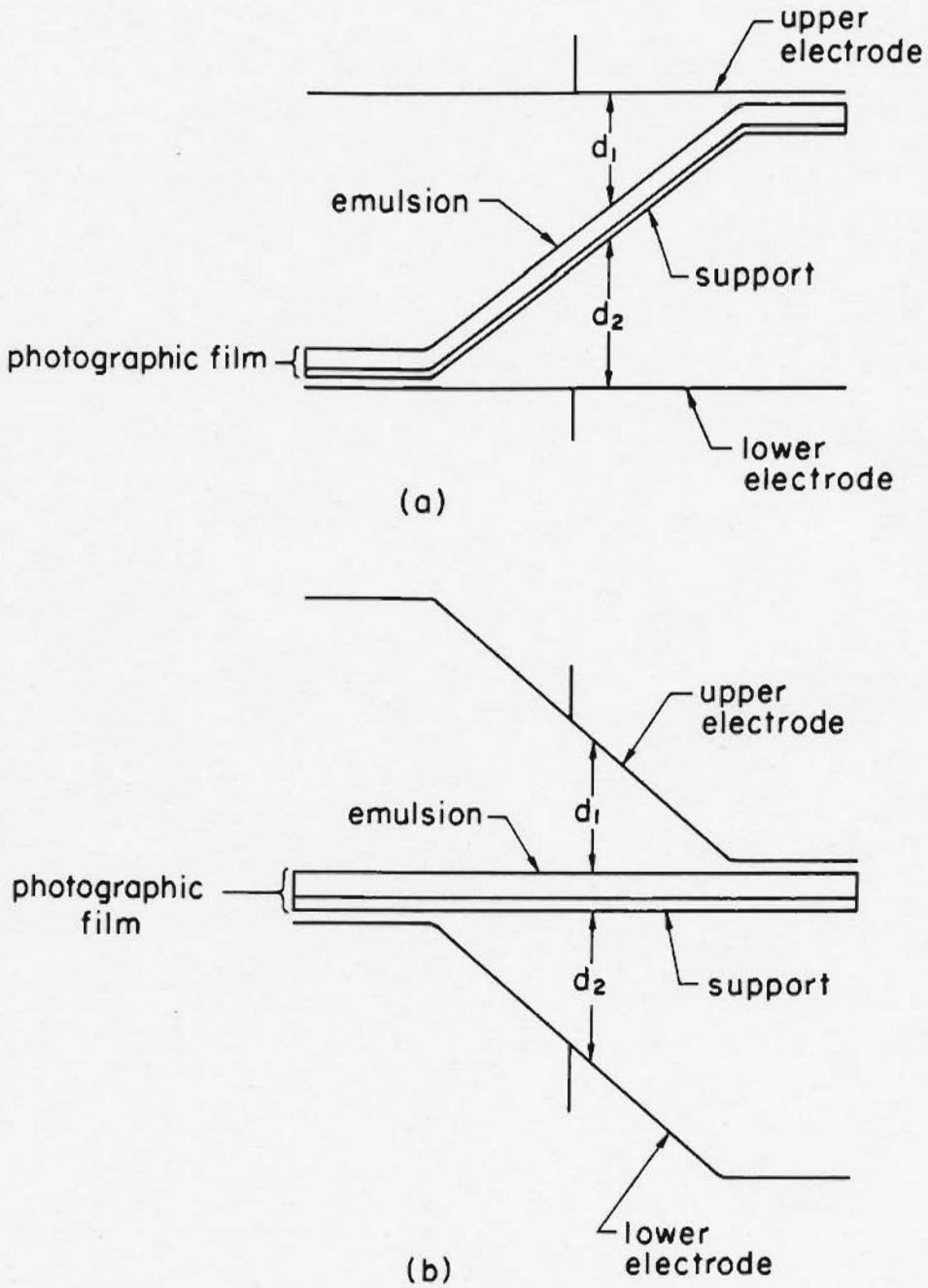
upper
electrode
d_1
emulsion
support
d_2
photographic film
lower
electrode
(a)
upper
electrode
emulsion
d_1
photographic
film
d_2
support
lower
electrode
(b)

FIGURE 13

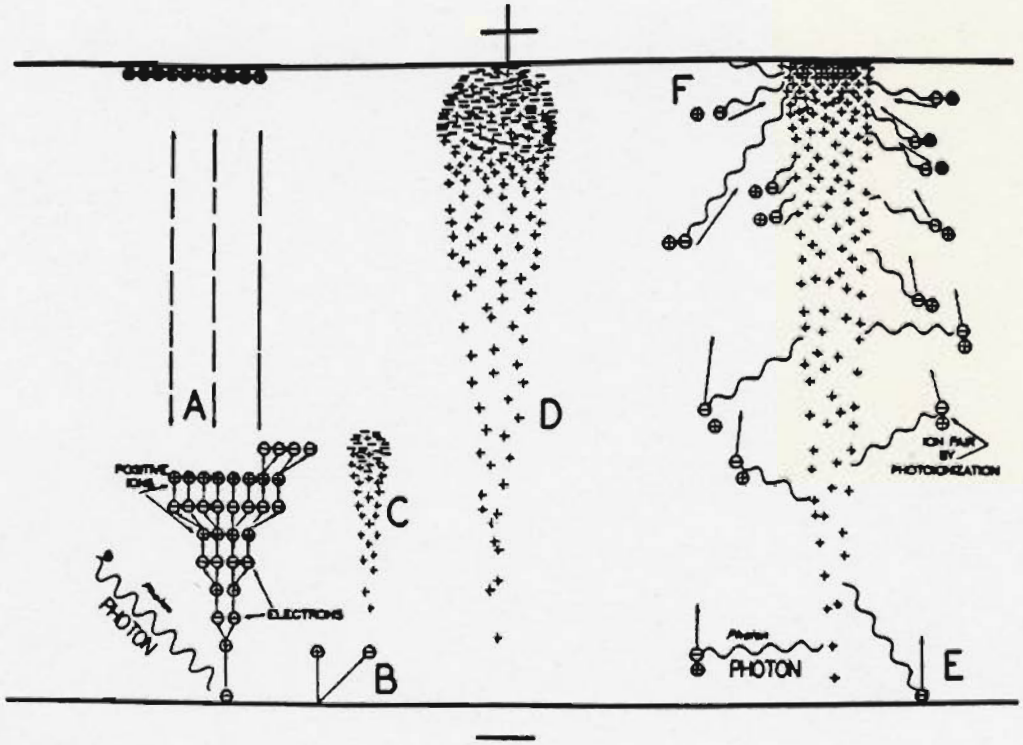

FIGURE 14

FIGURE 15

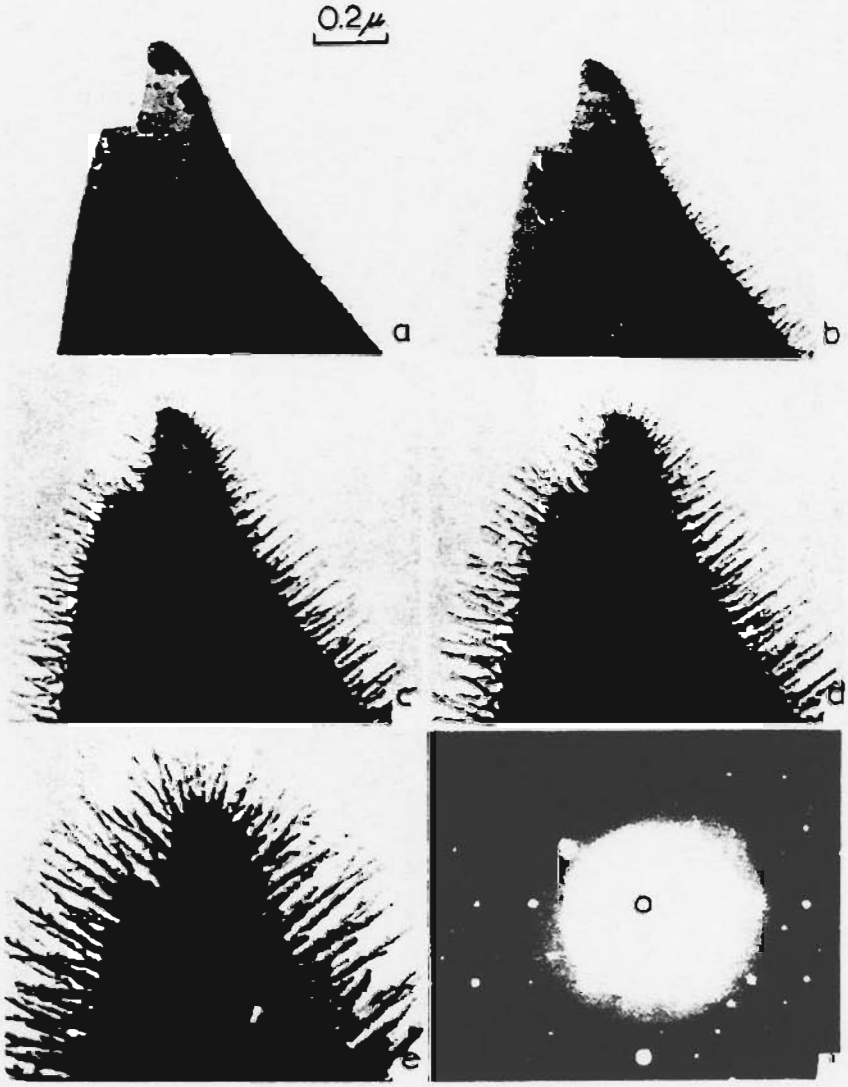

FIGURE 16

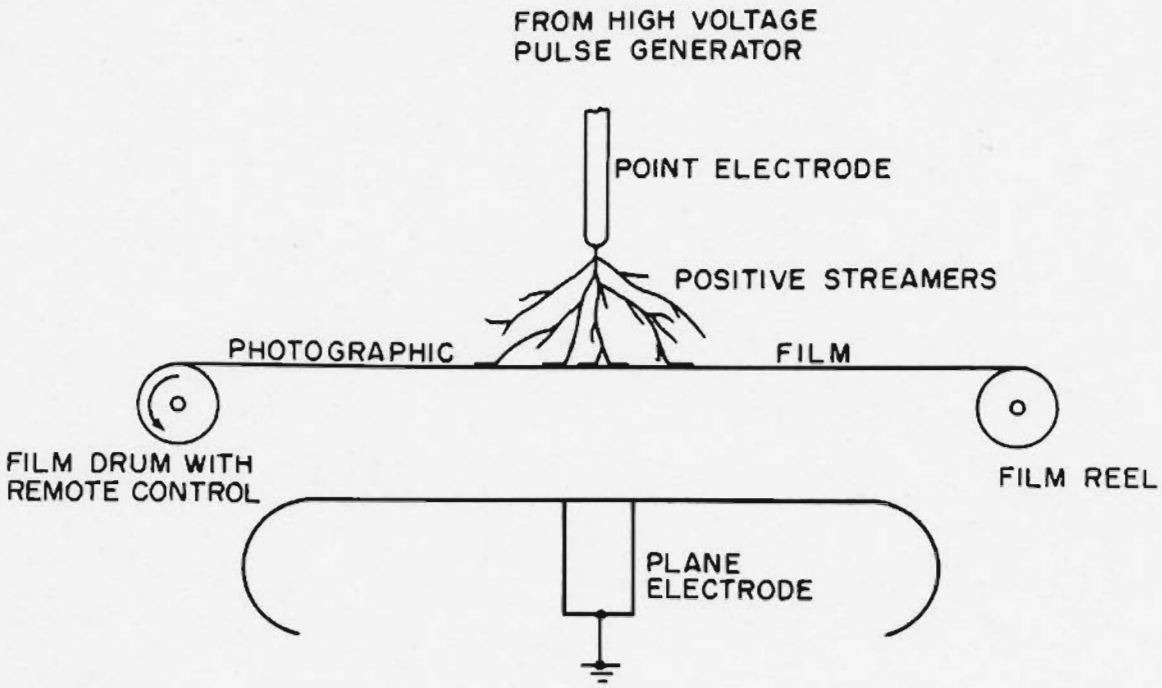

FIGURE 17

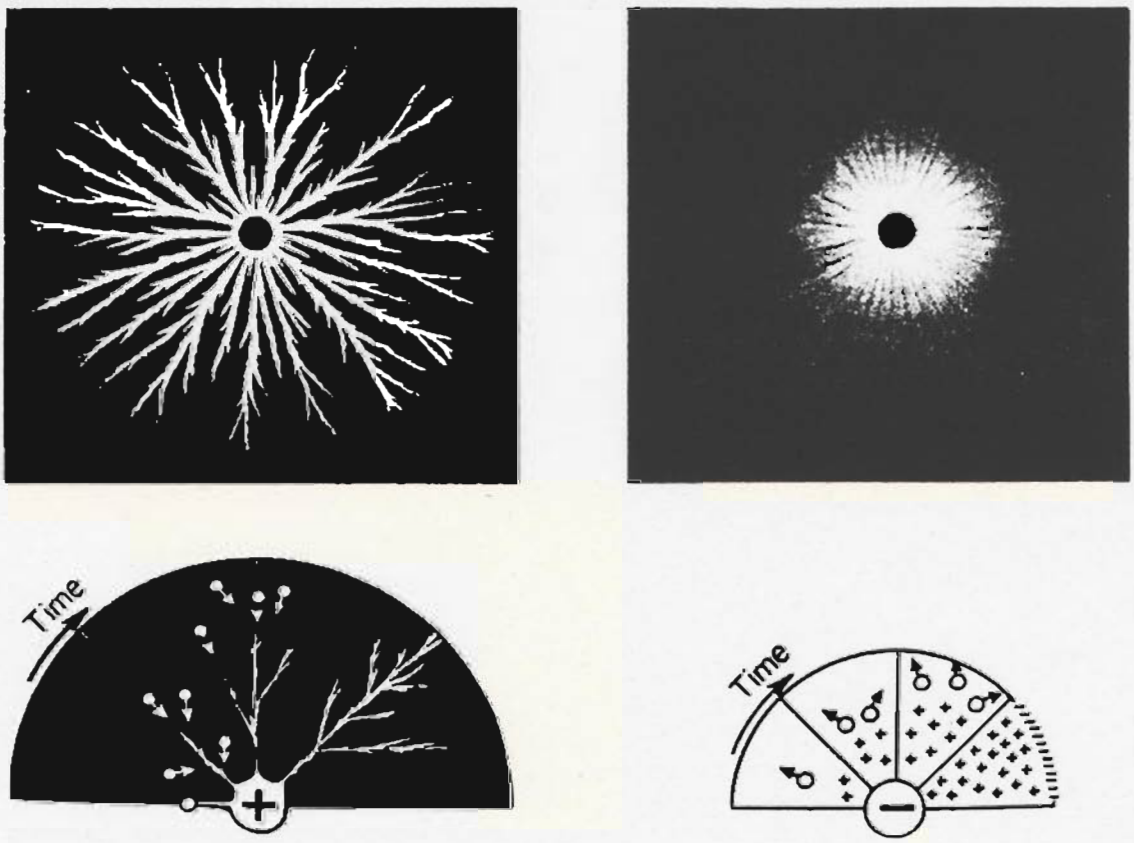

FIGURE 18

FIGURE 19

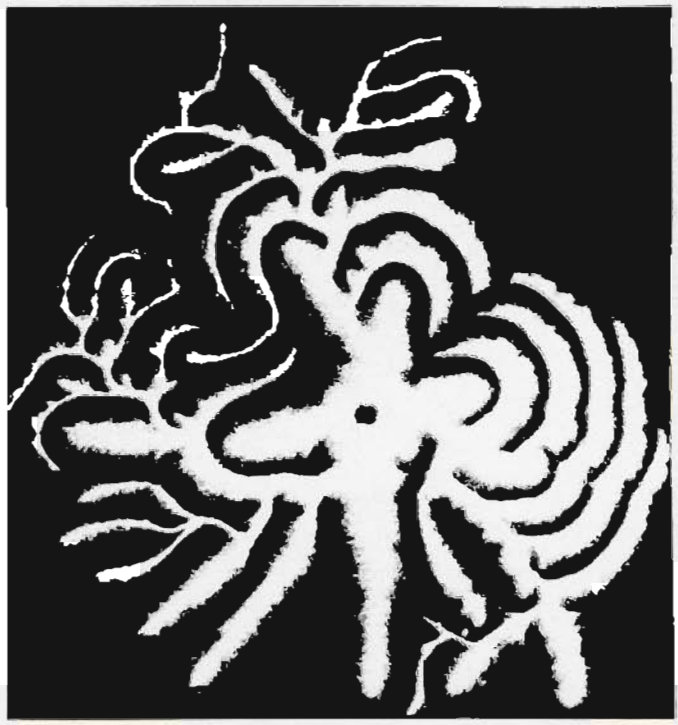

FIGURE 20

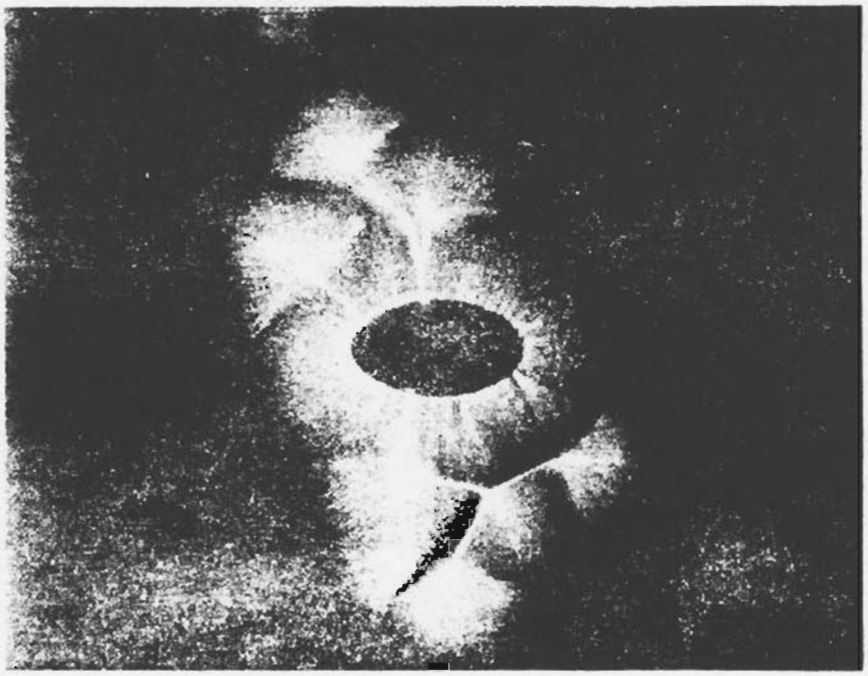

FIGURE 21

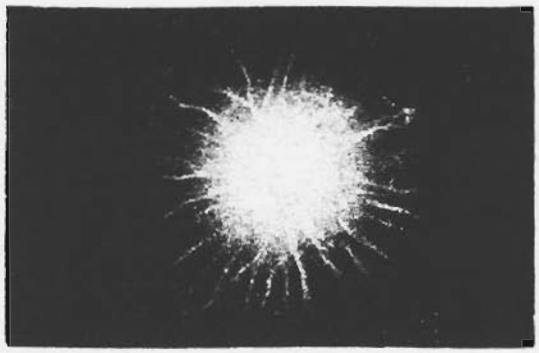

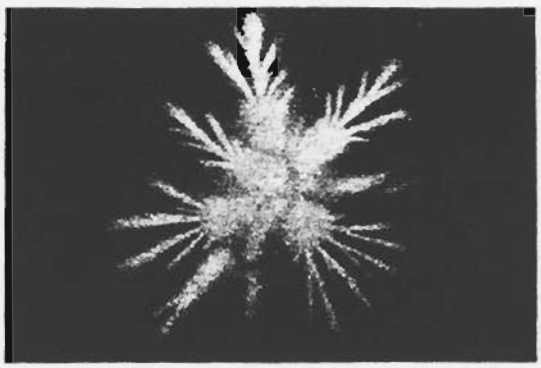

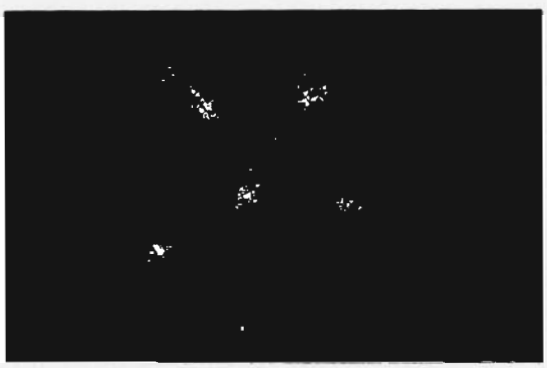

FIGURE 22

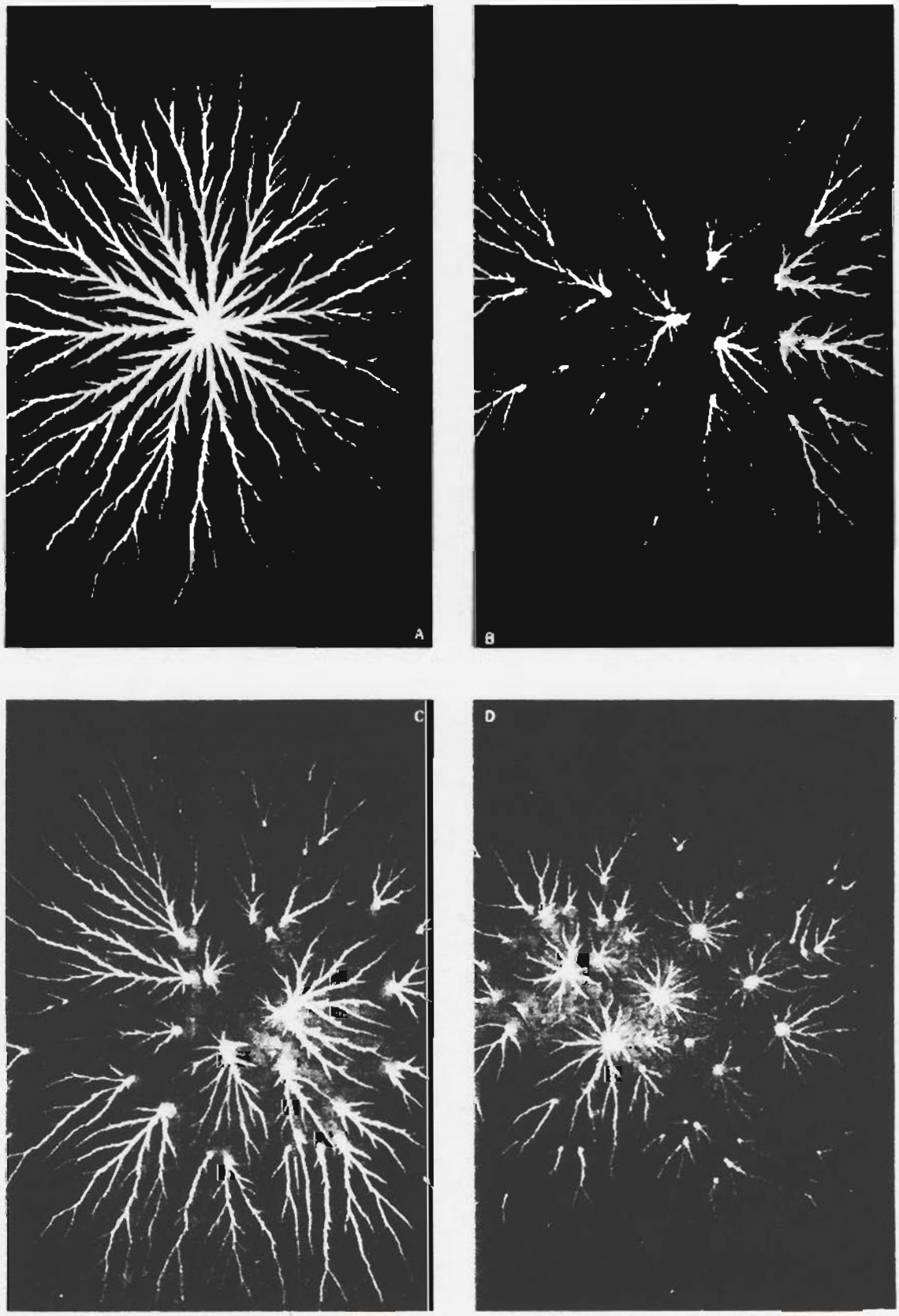

FIGURE 23

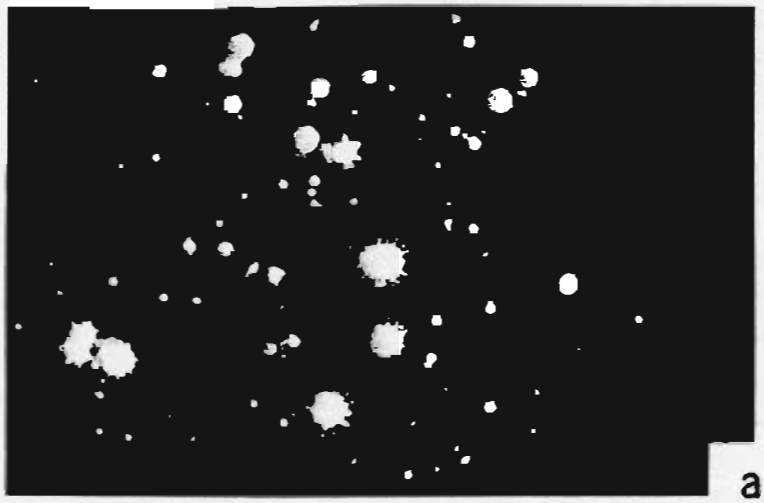

a

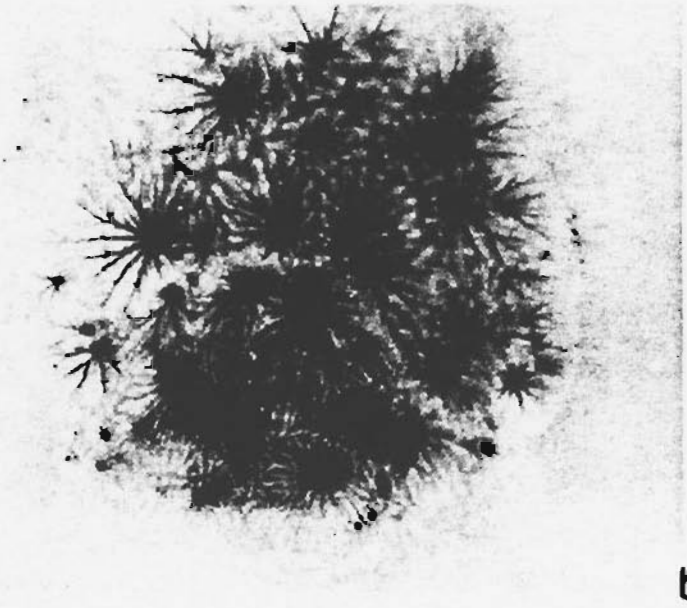

b

FIGURE 24

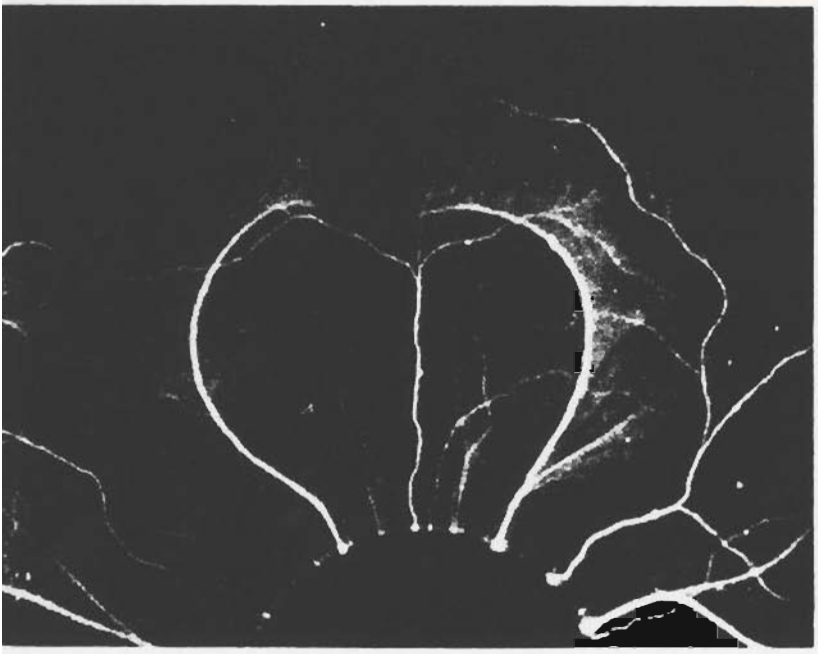

FIGURE 25

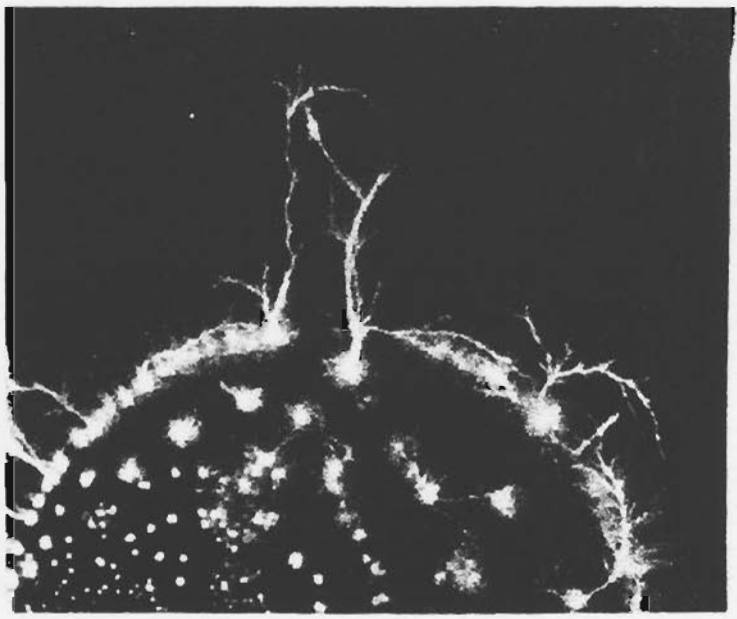

FIGURE 26

FIGURE 27

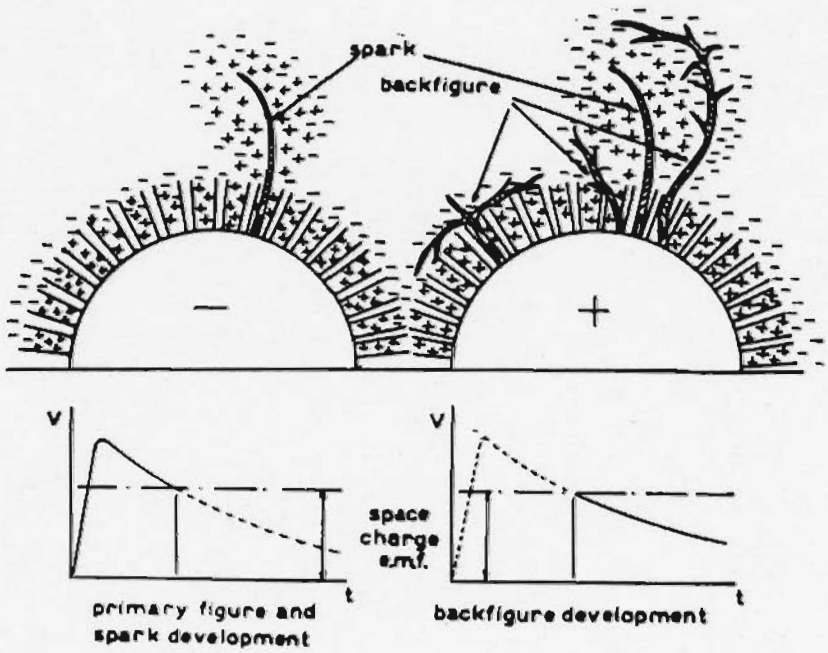

FIGURE 28

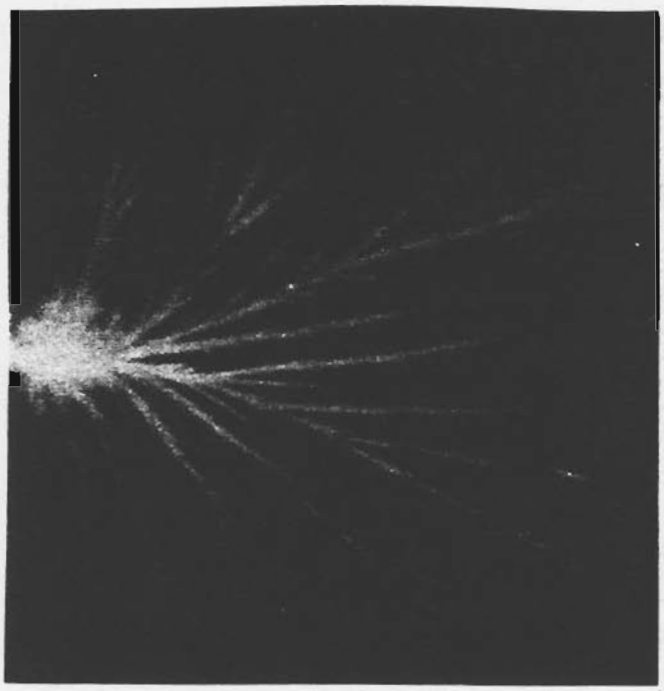

FIGURE 29

FIGURE 30

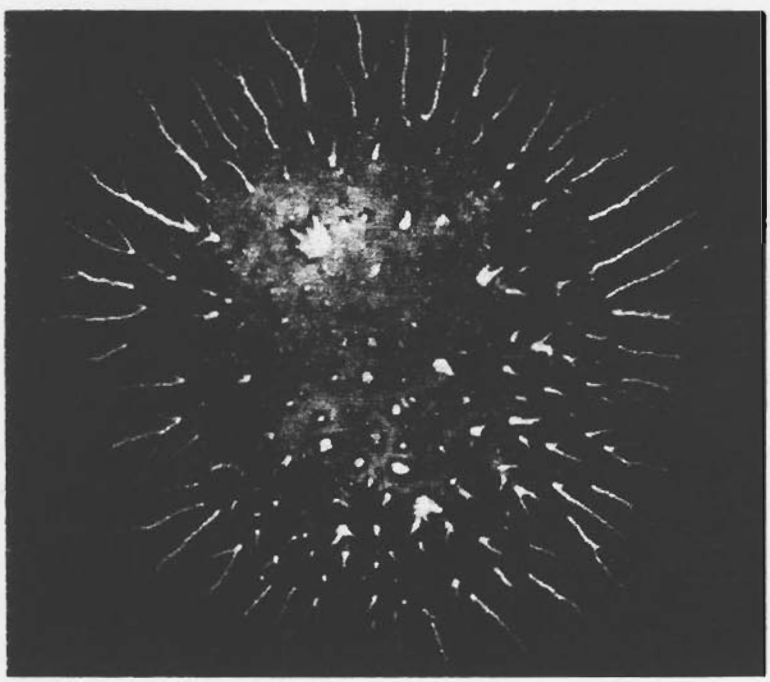

FIGURE 31

FIGURE 32

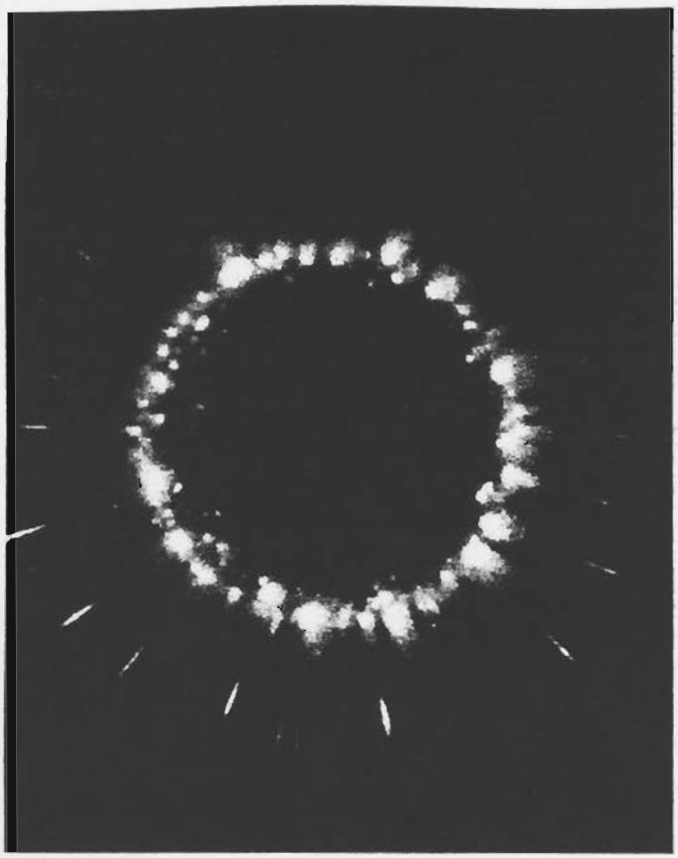

FIGURE 33a

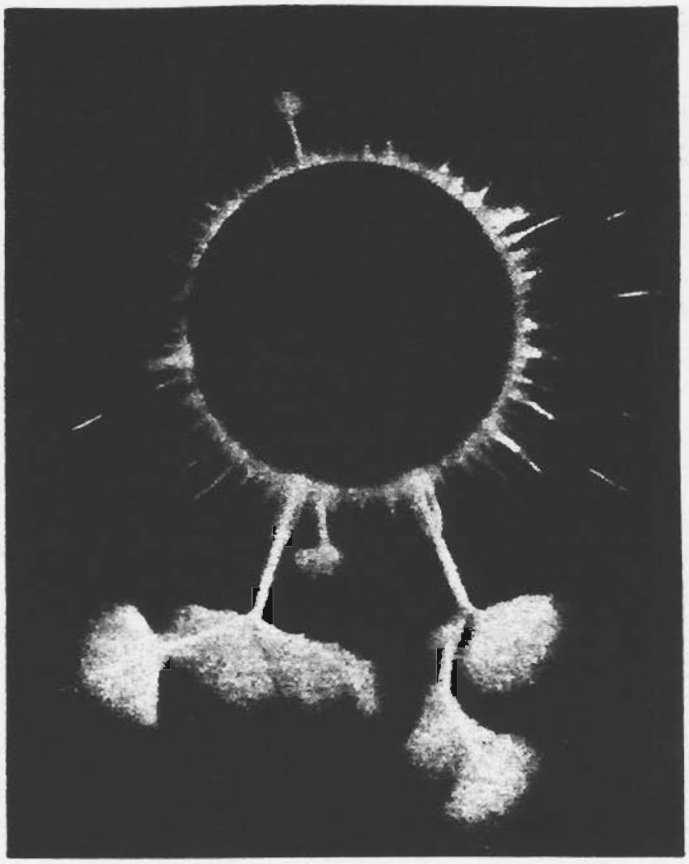

FIGURE 33b

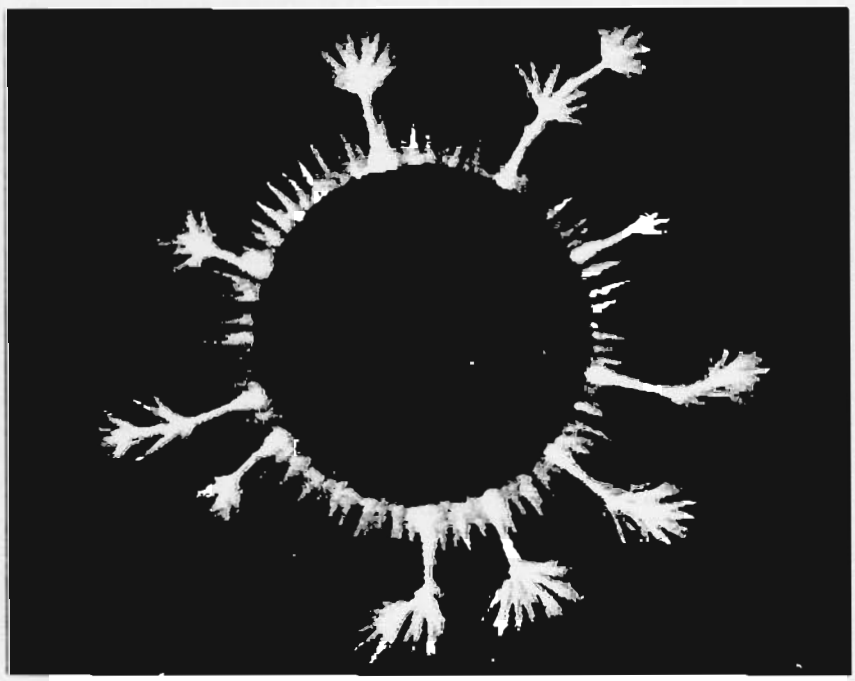

FIGURE 34

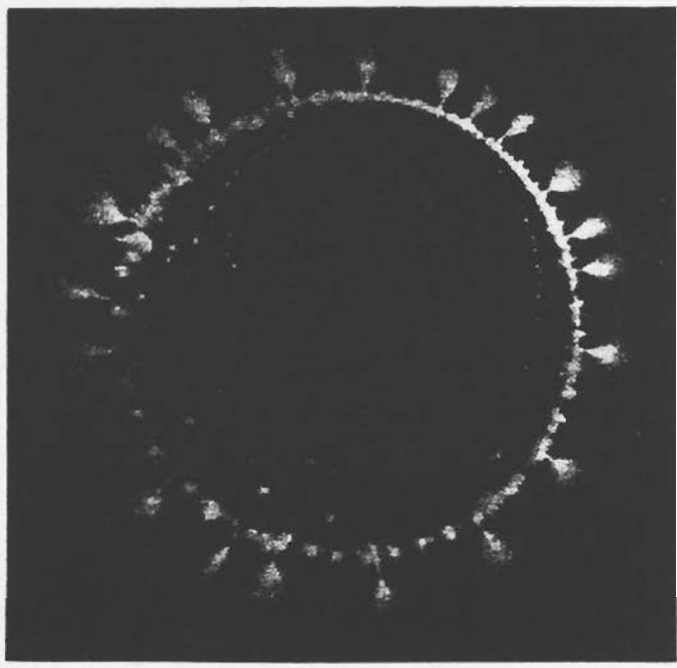

FIGURE 35

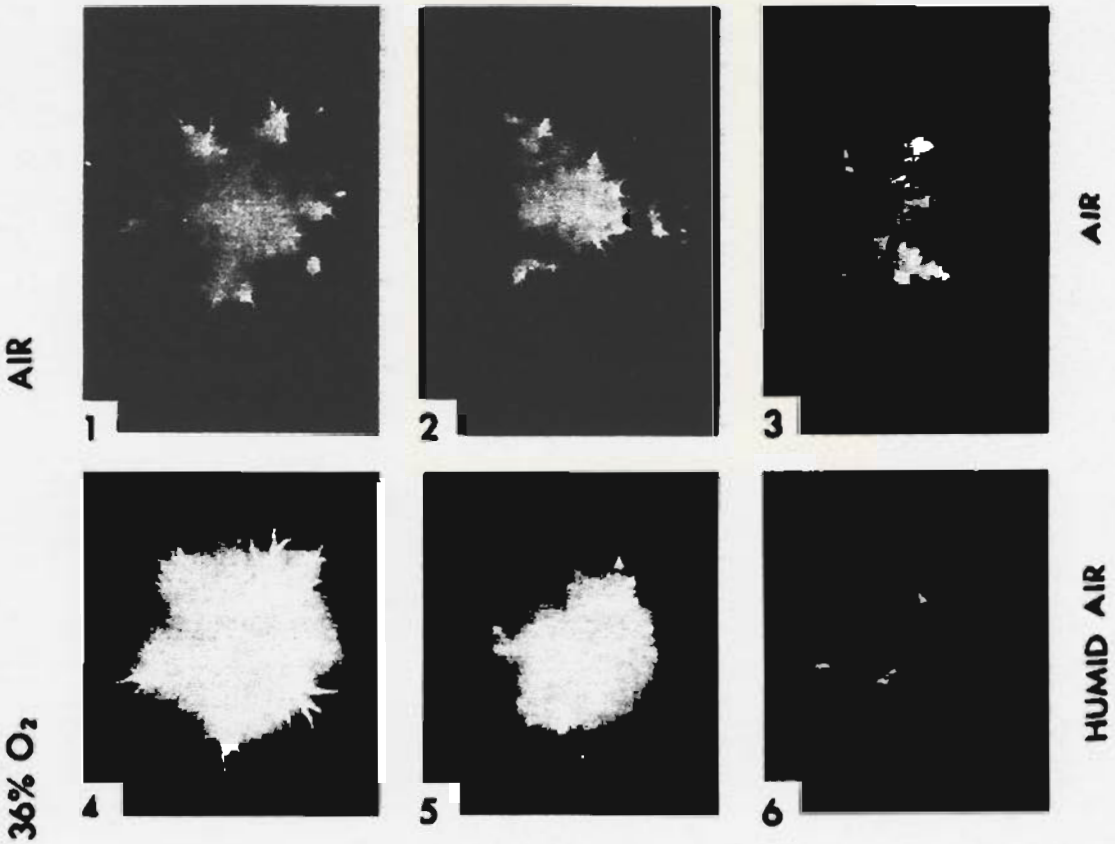

FIGURE 36

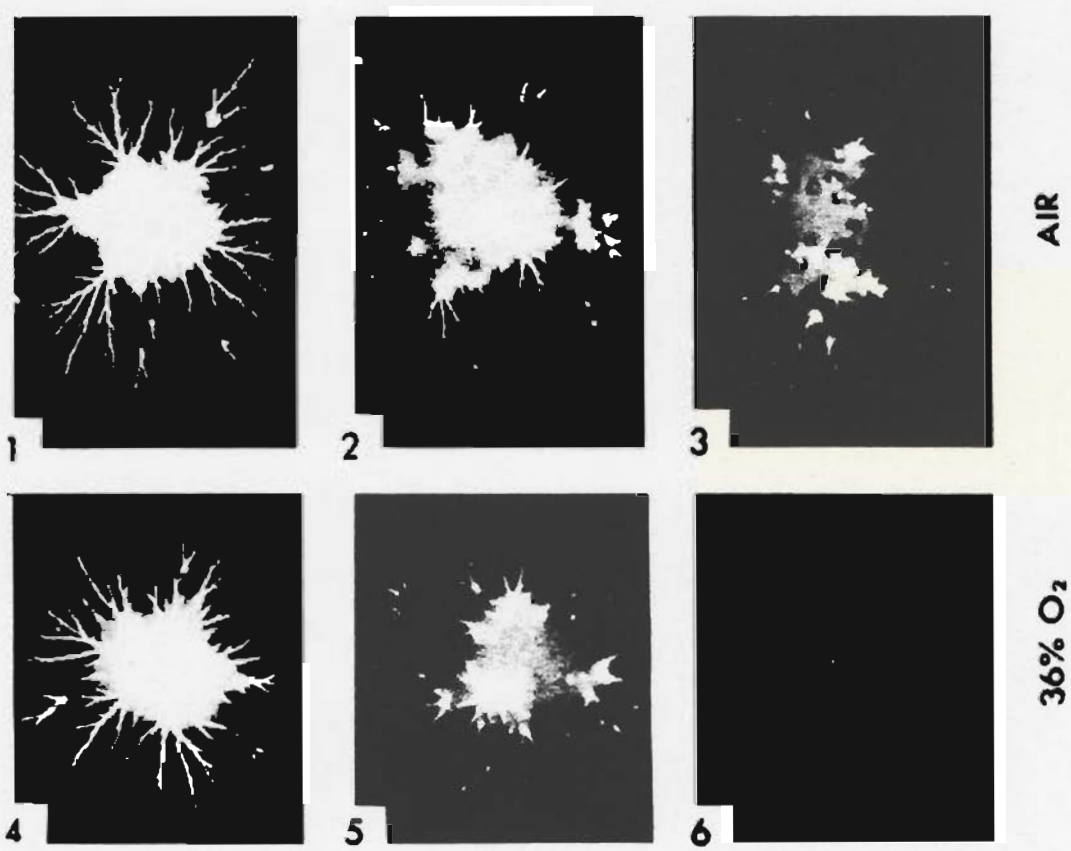

FIGURE 37

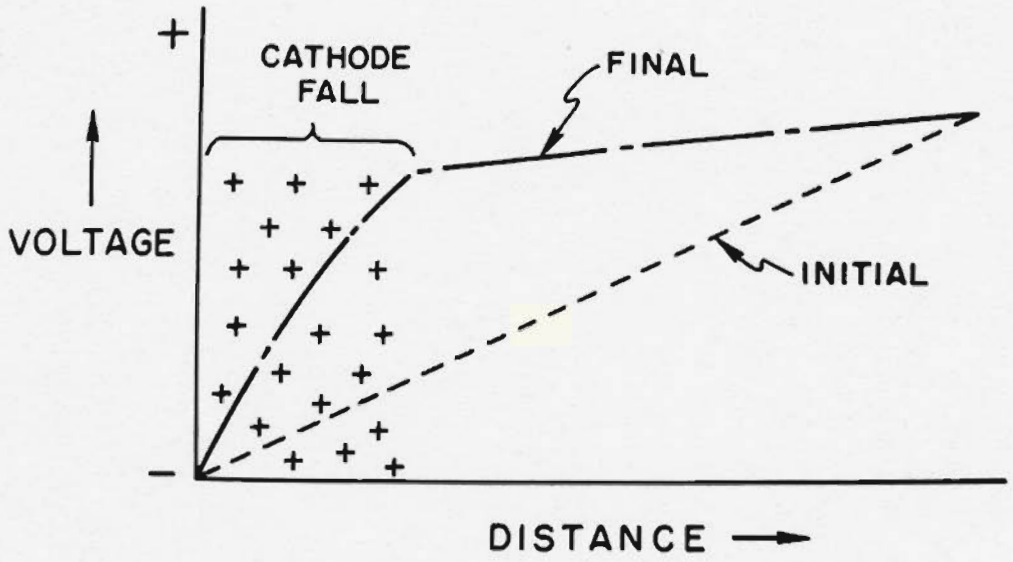

FIGURE 38

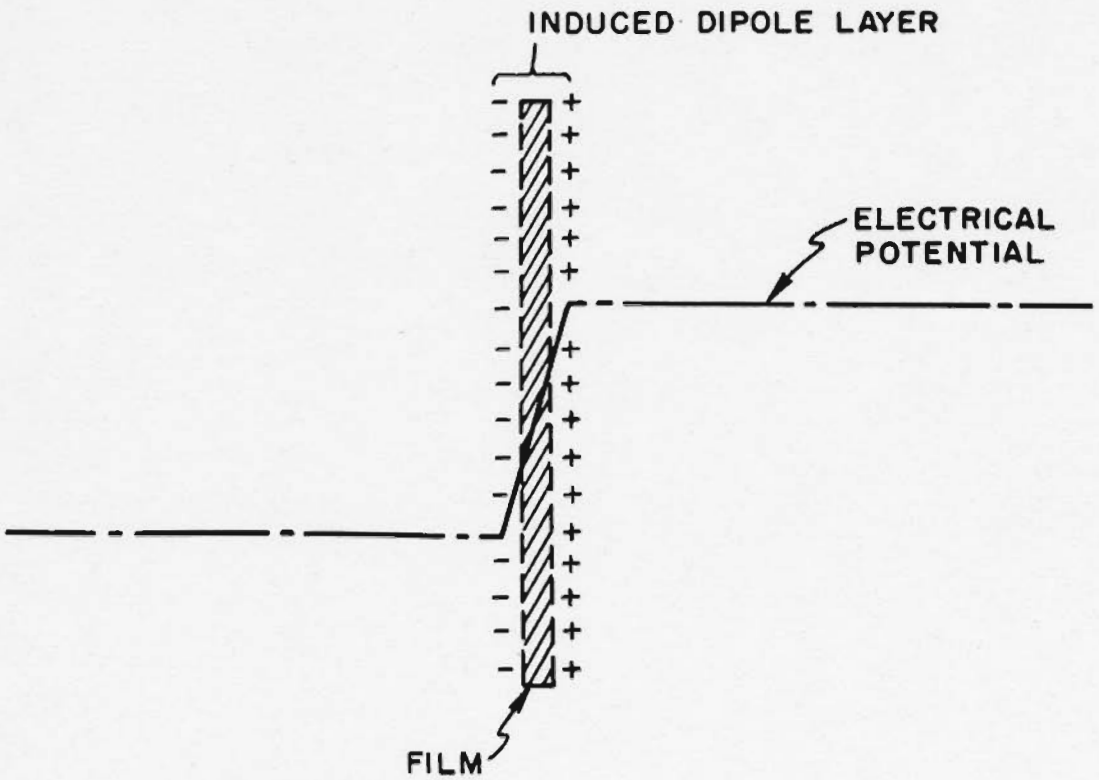

FIGURE 39

The Light Source in High-Voltage Photography

The attached figures are better reproductions of those already bound into the report.

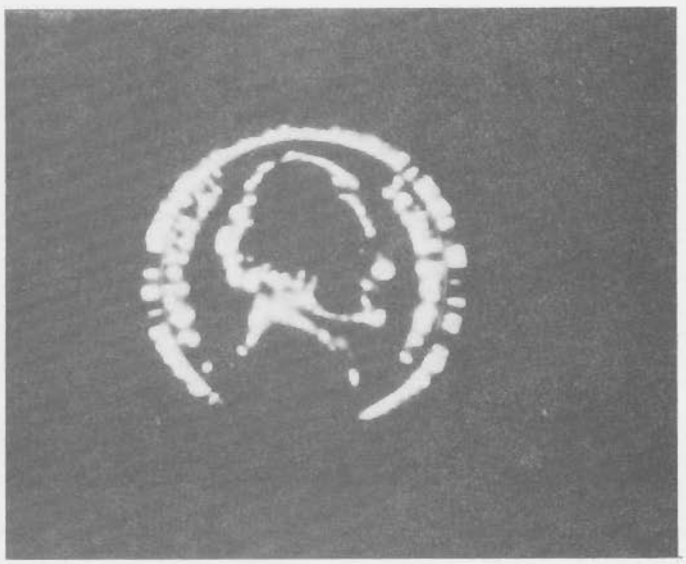

(a)

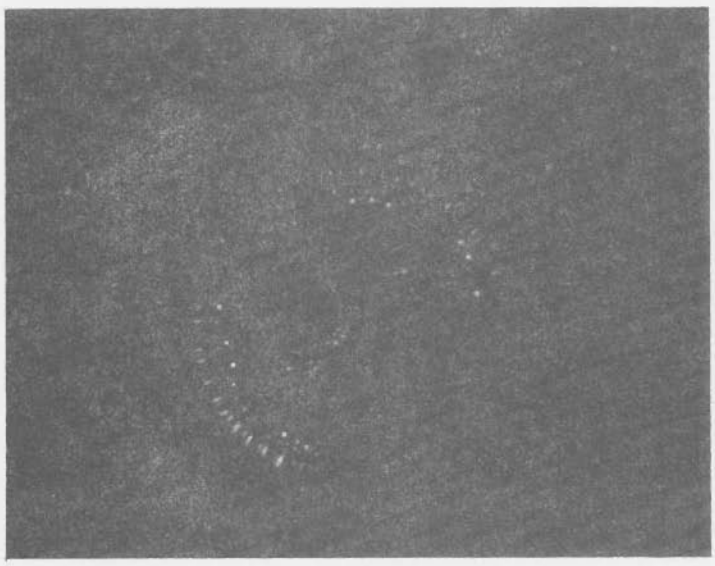

(b)

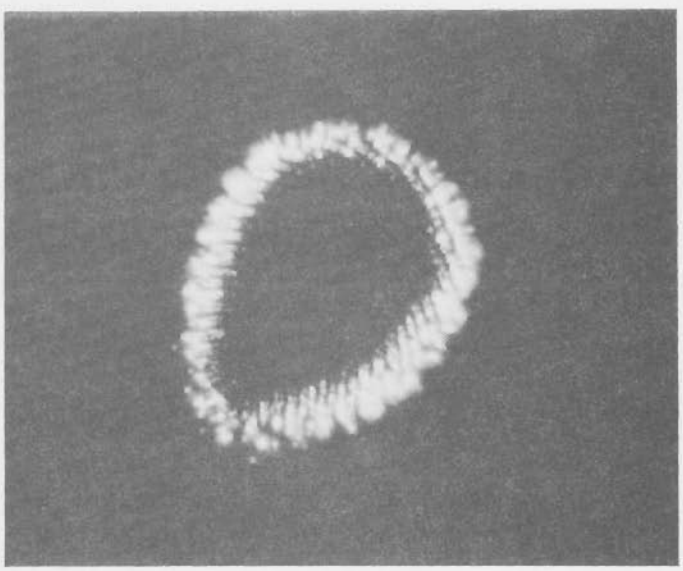

(c)

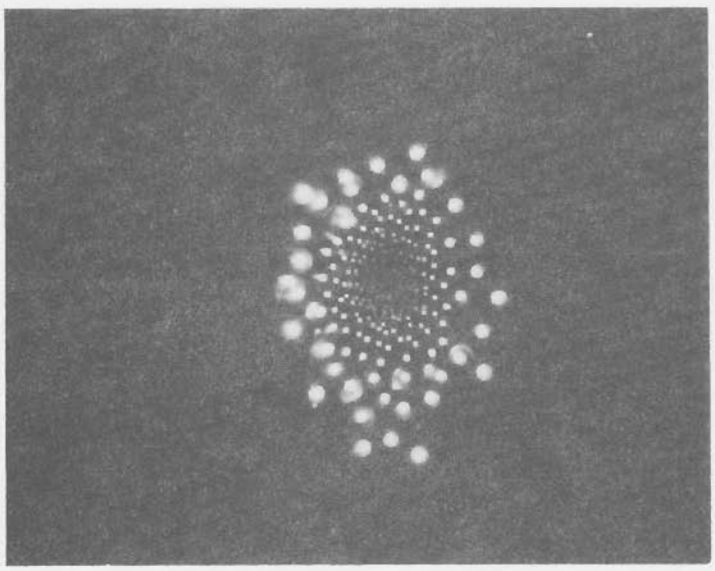

(d)

FIGURE 10

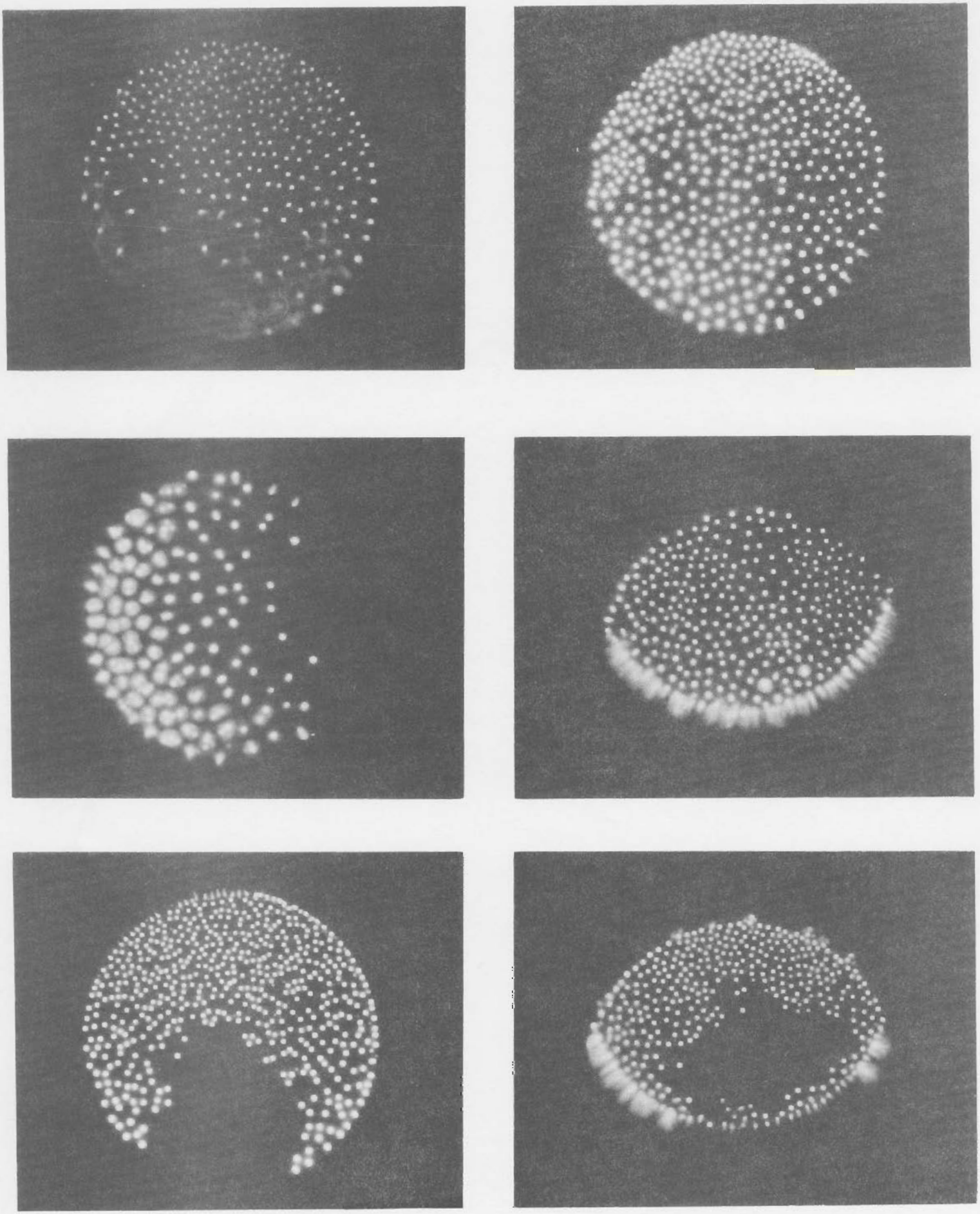

FIGURE 11

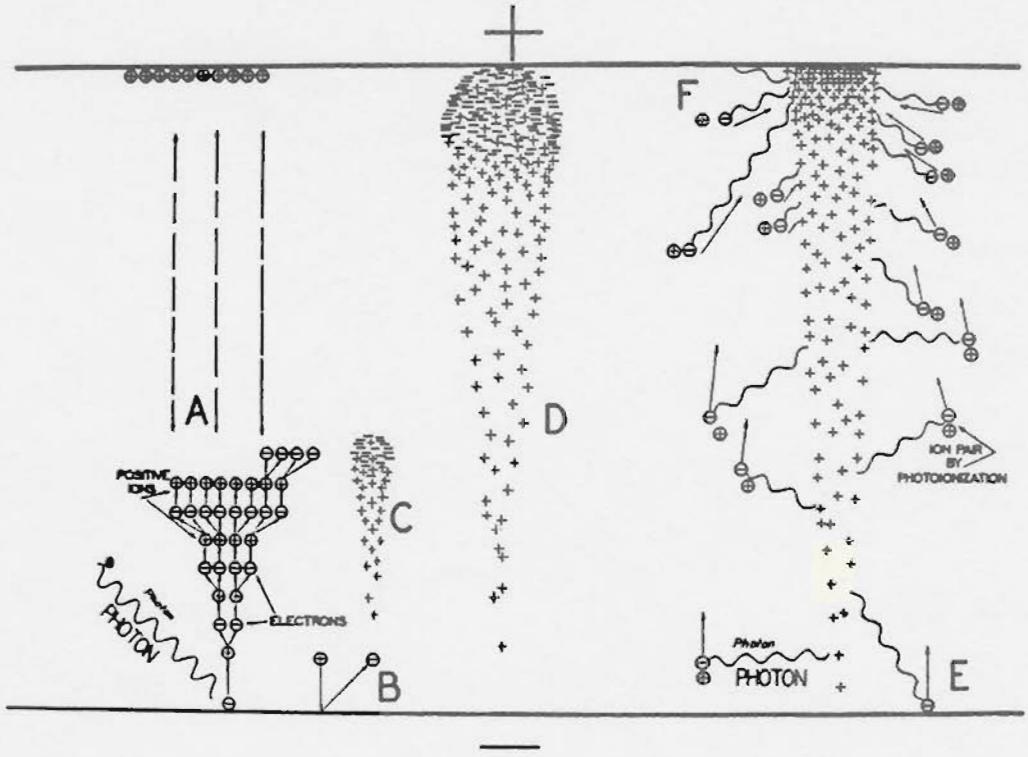

FIGURE 14

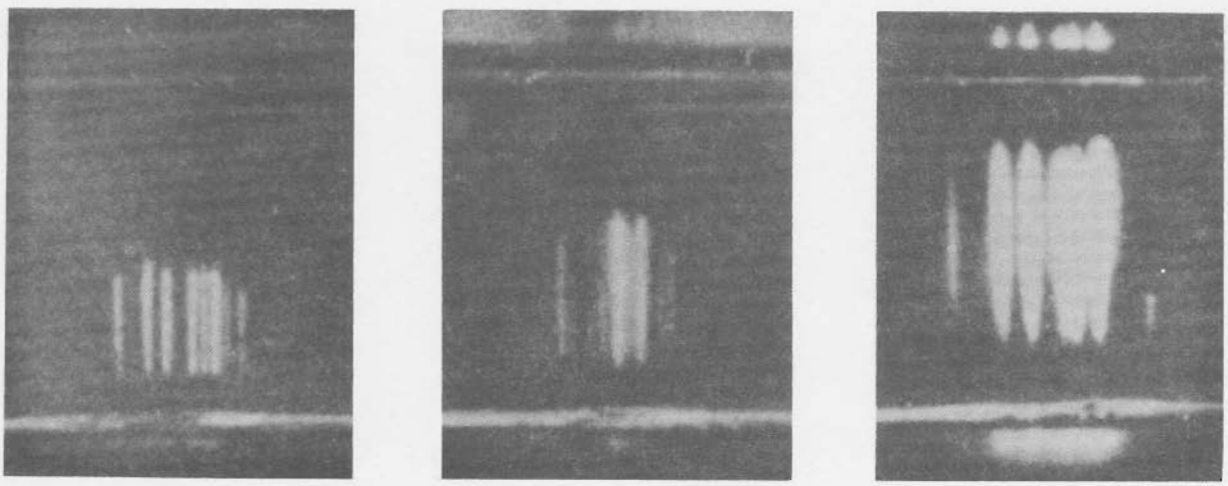

FIGURE 15

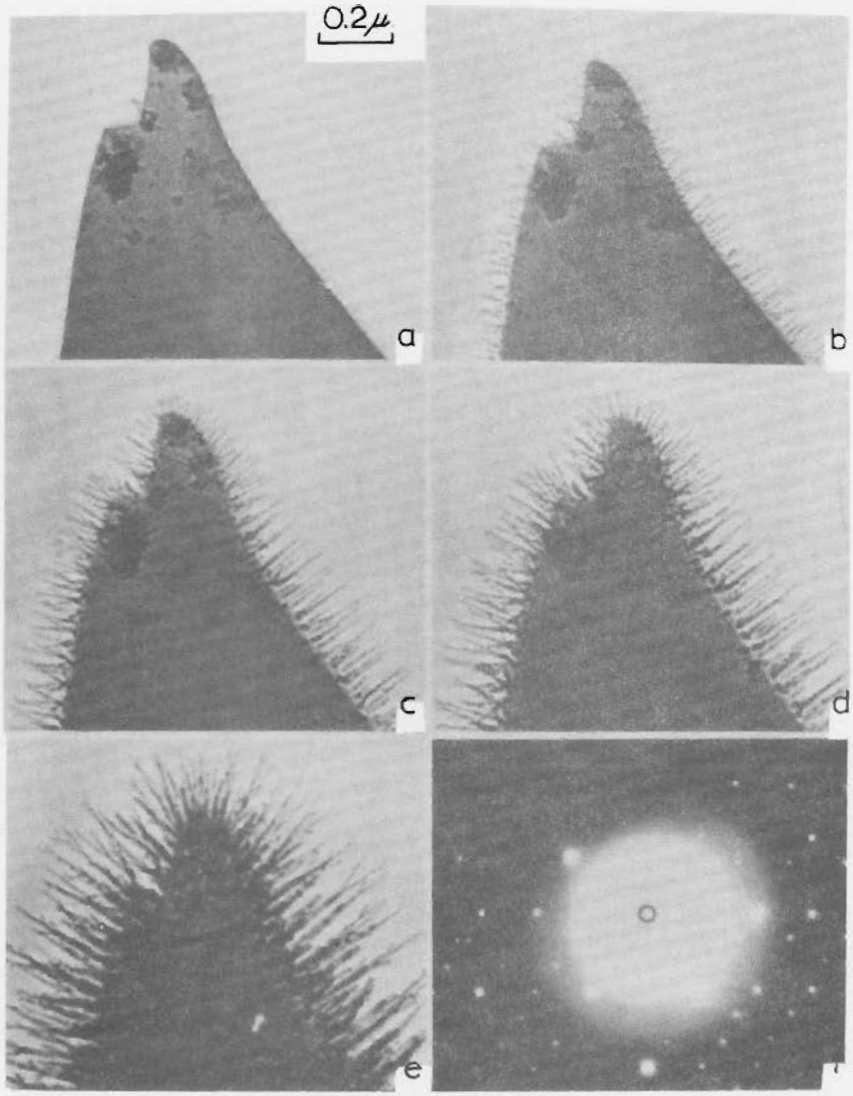

FIGURE 16

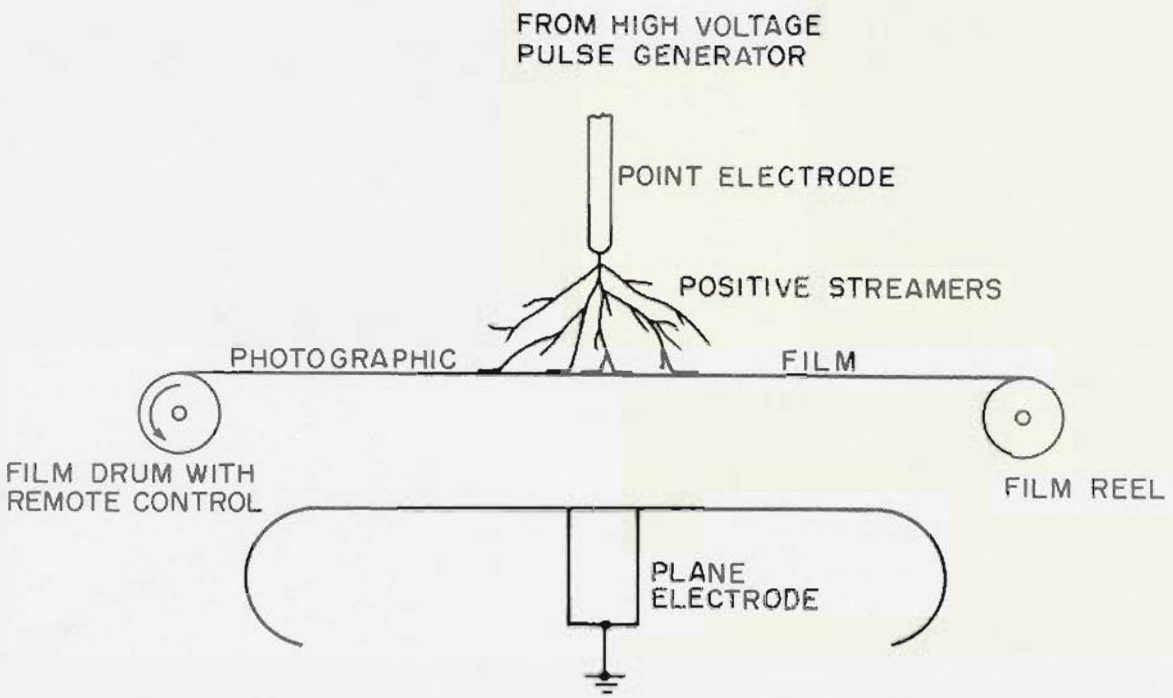

FIGURE 17

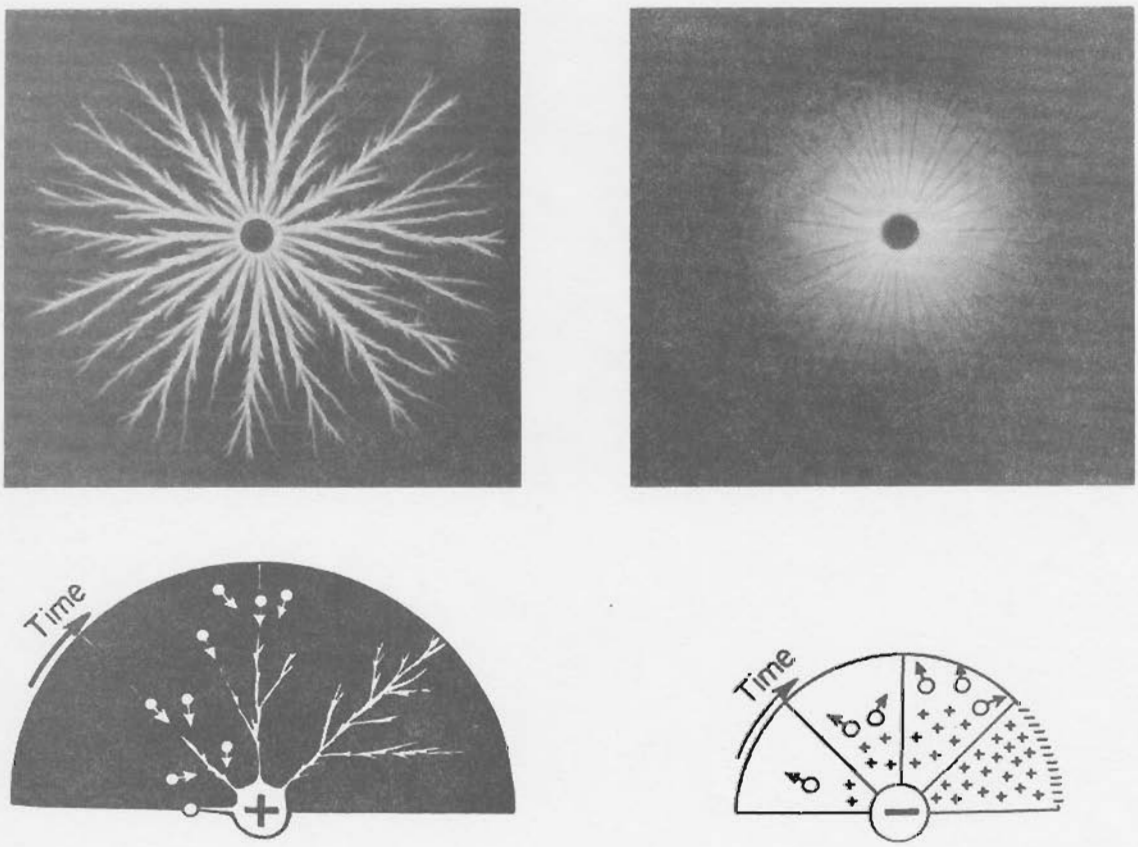

FIGURE 18

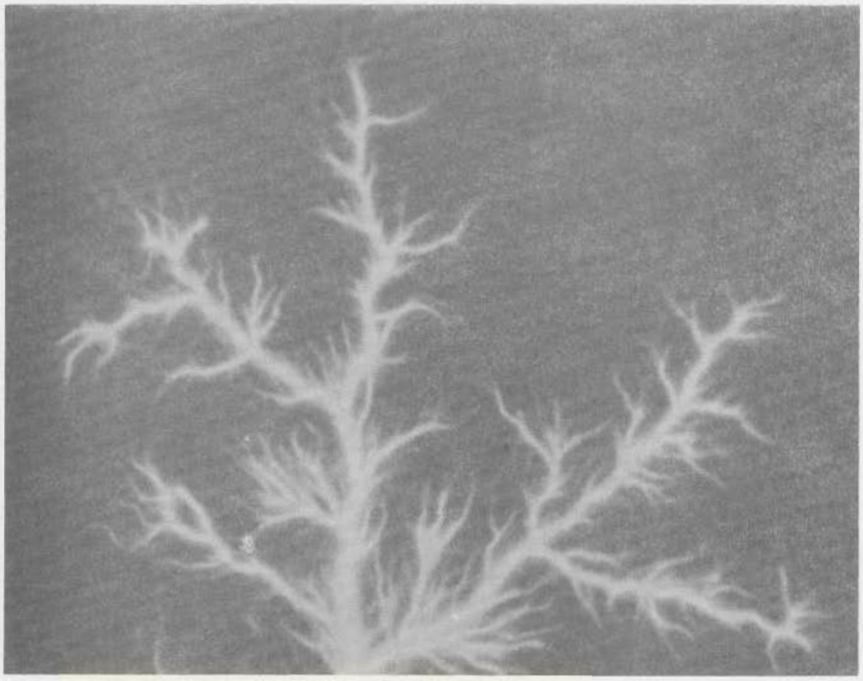

FIGURE 19

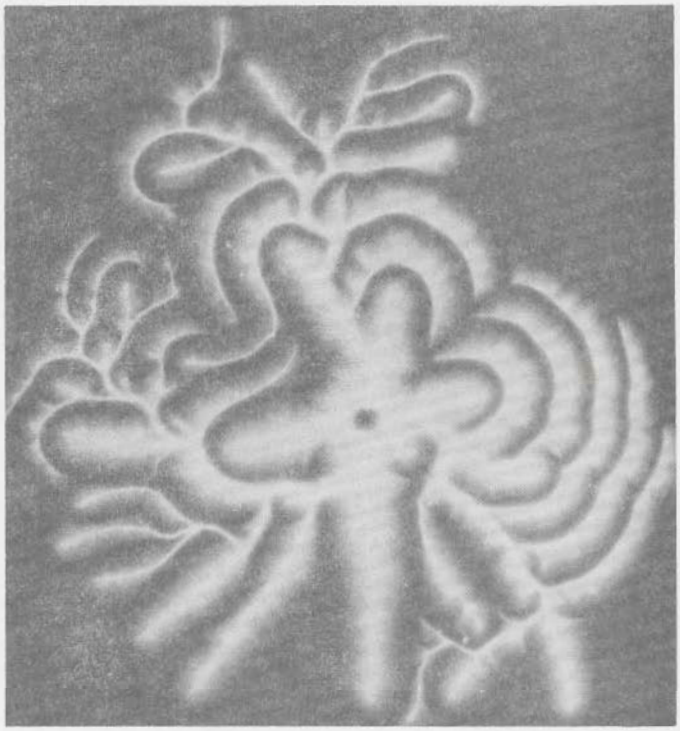

FIGURE 20

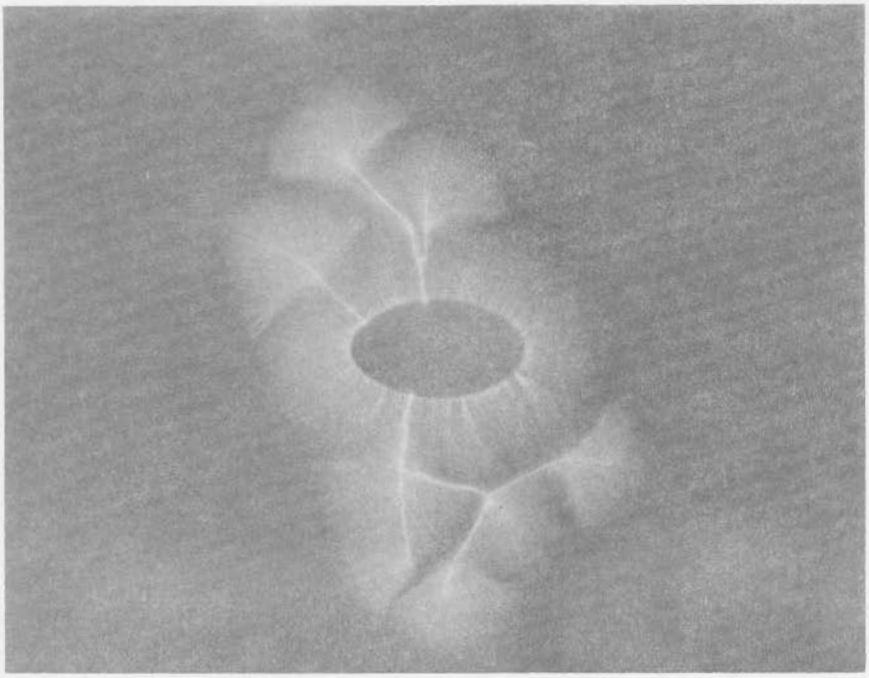

FIGURE 21

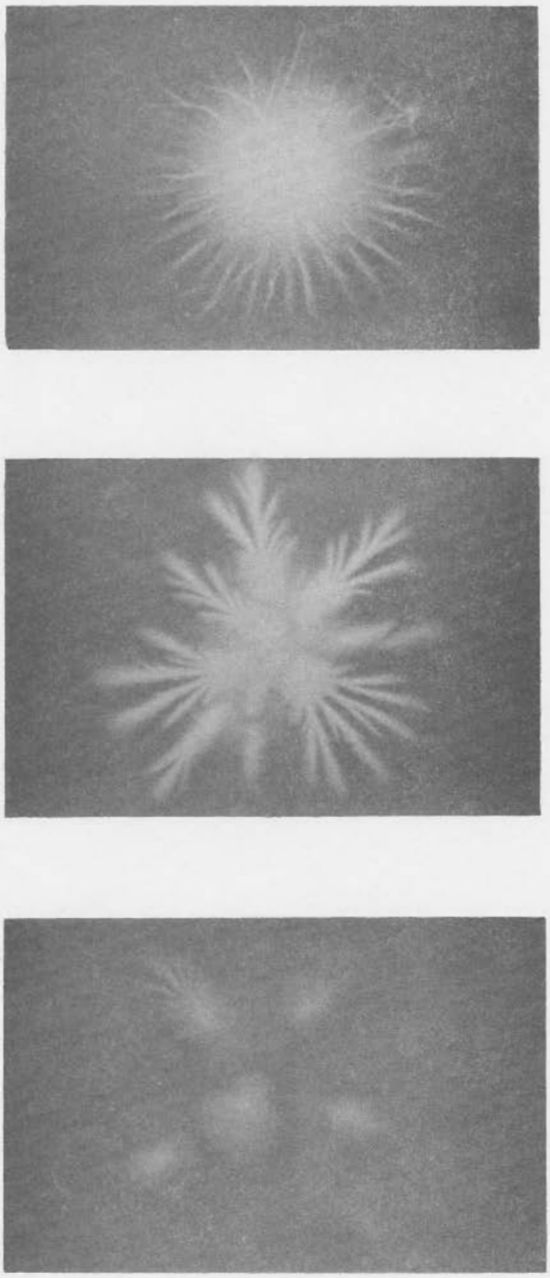

FIGURE 22

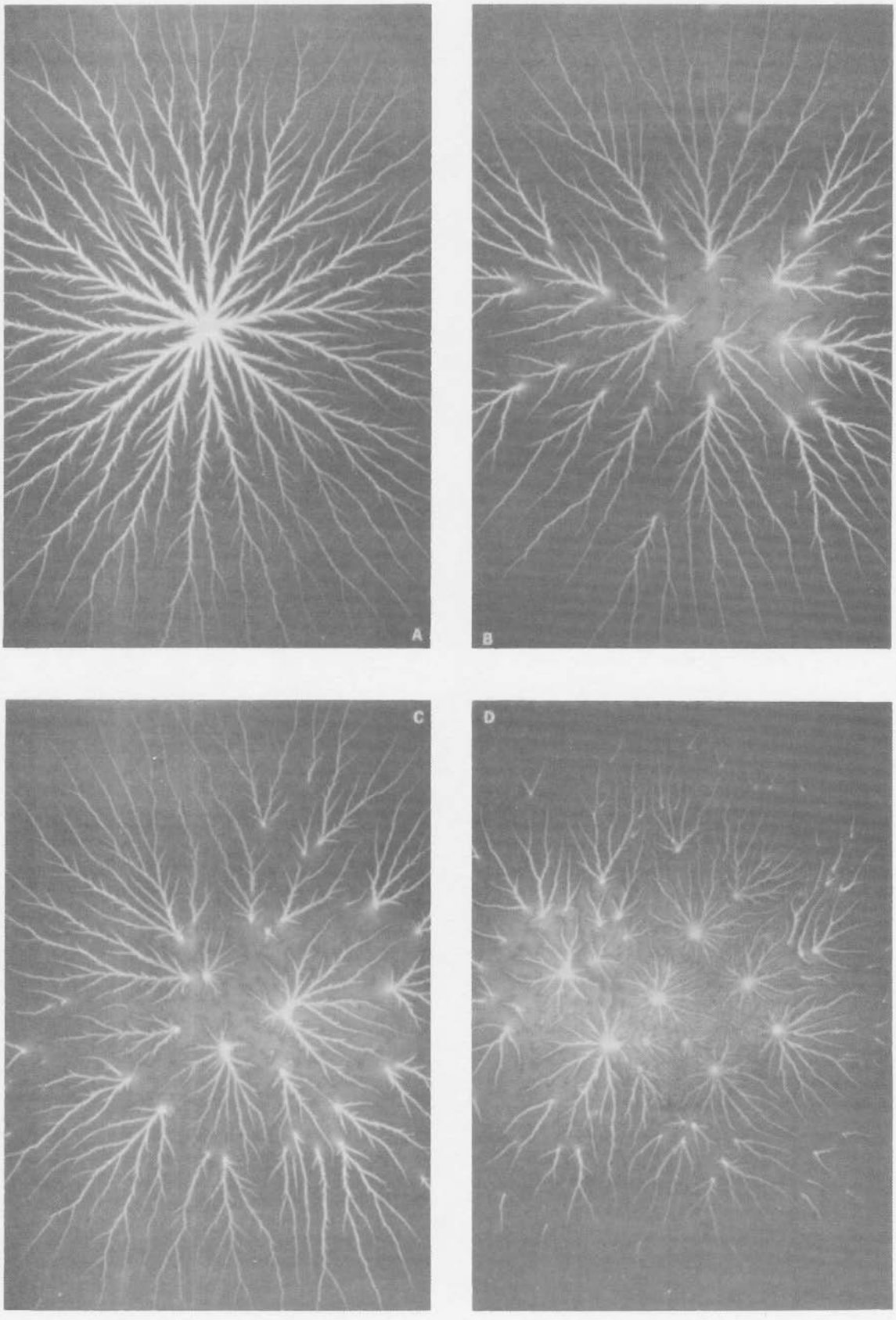

FIGURE 23

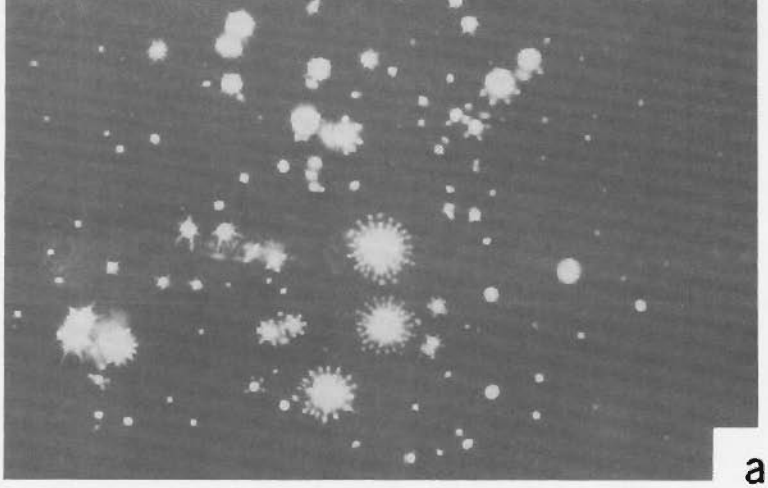

a

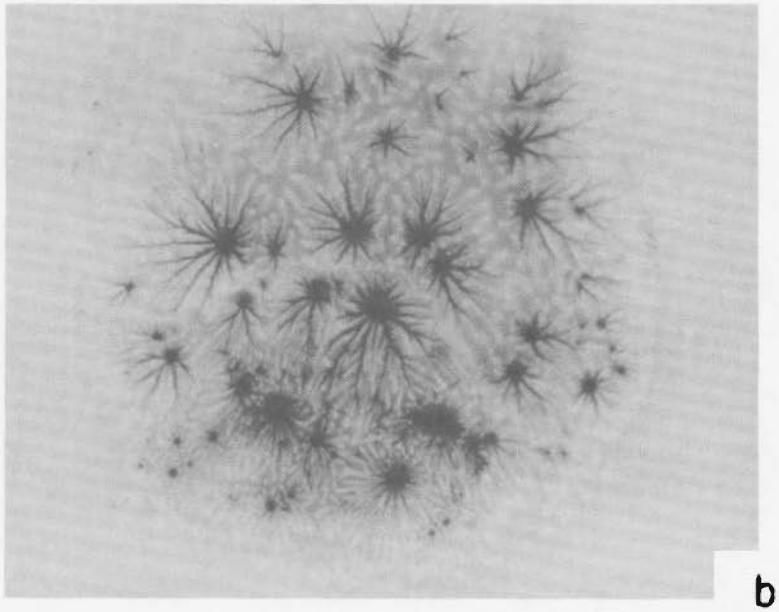

b

FIGURE 24

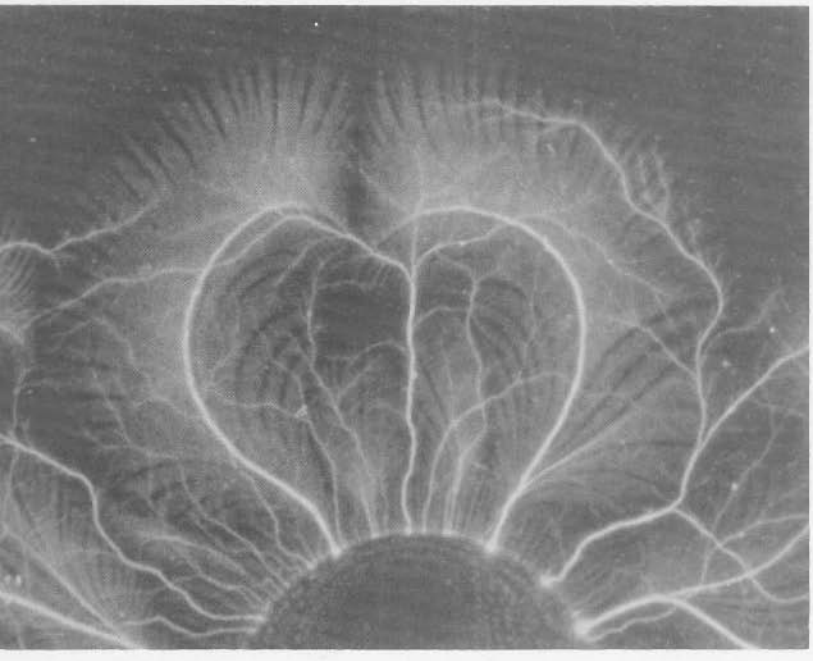

FIGURE 25

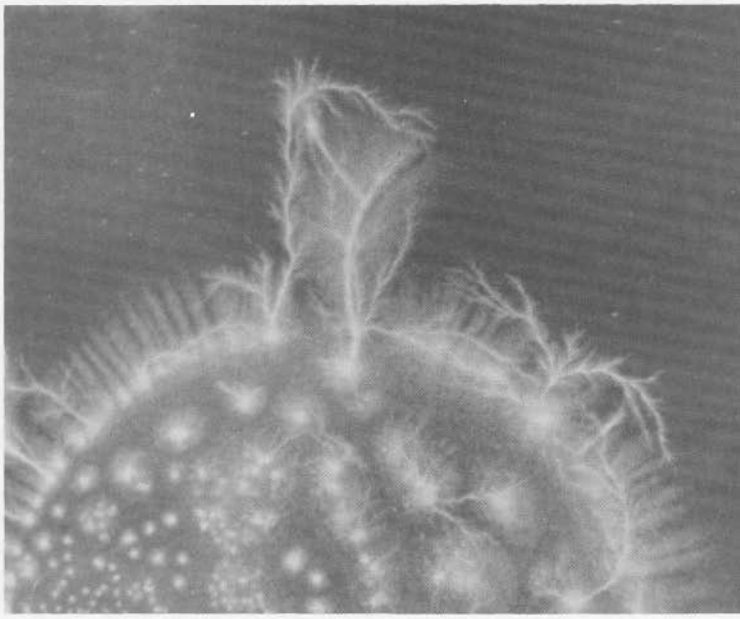

FIGURE 26

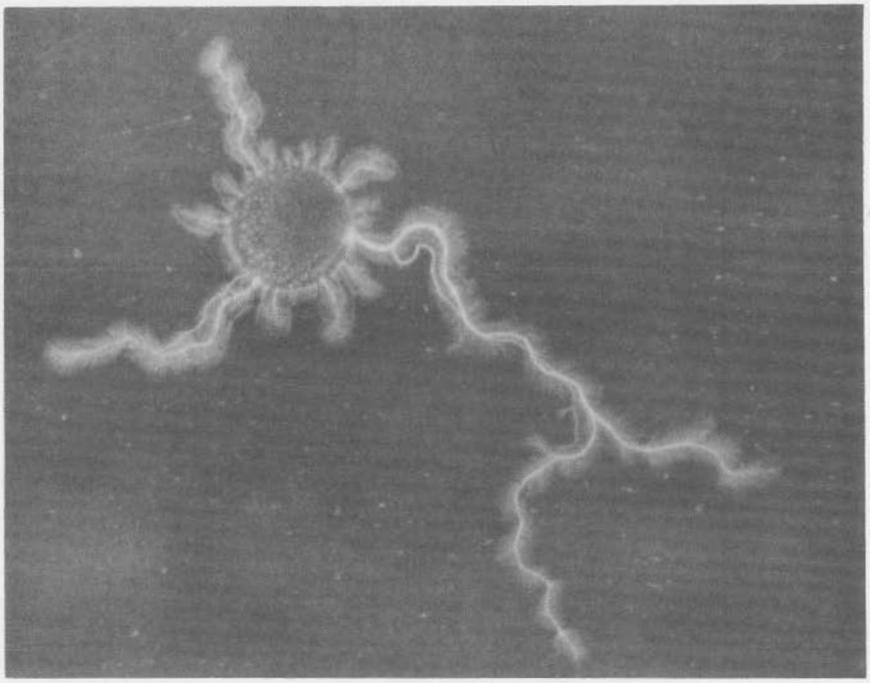

FIGURE 27

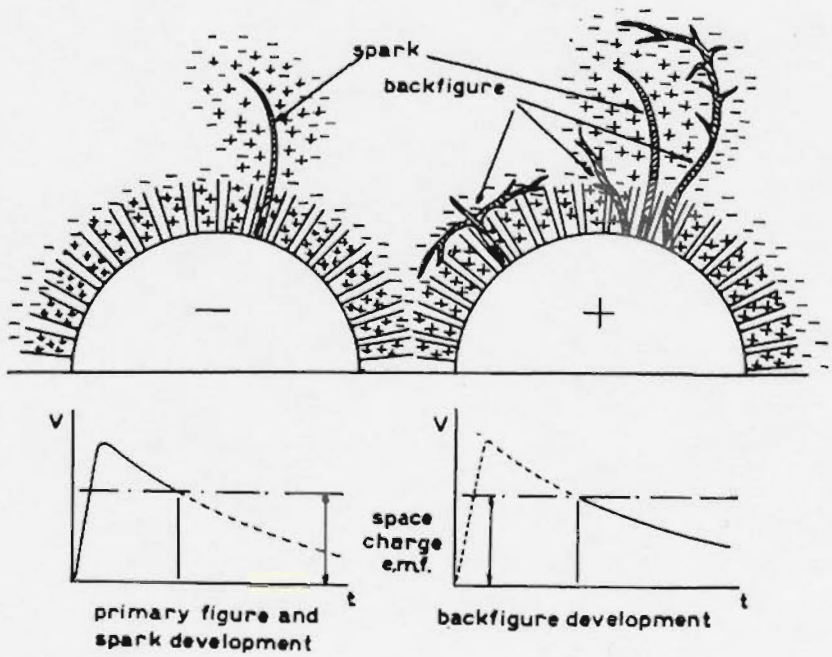

FIGURE 28

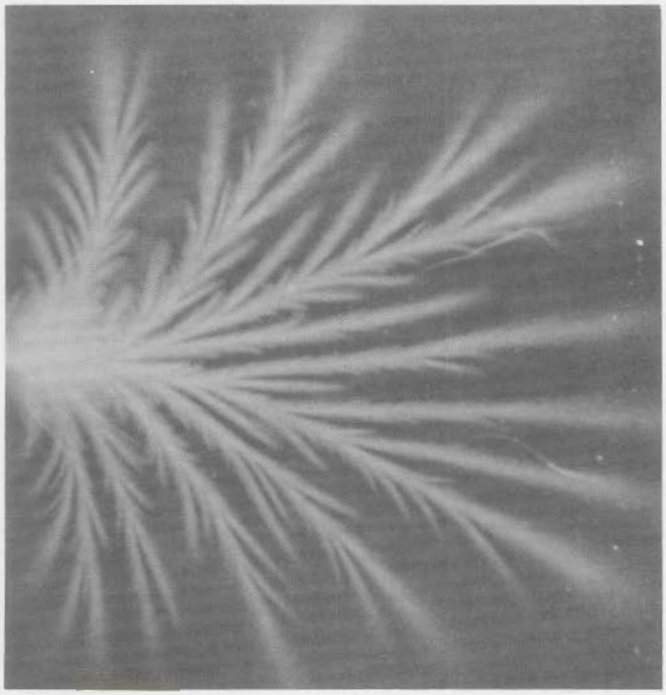

FIGURE 29

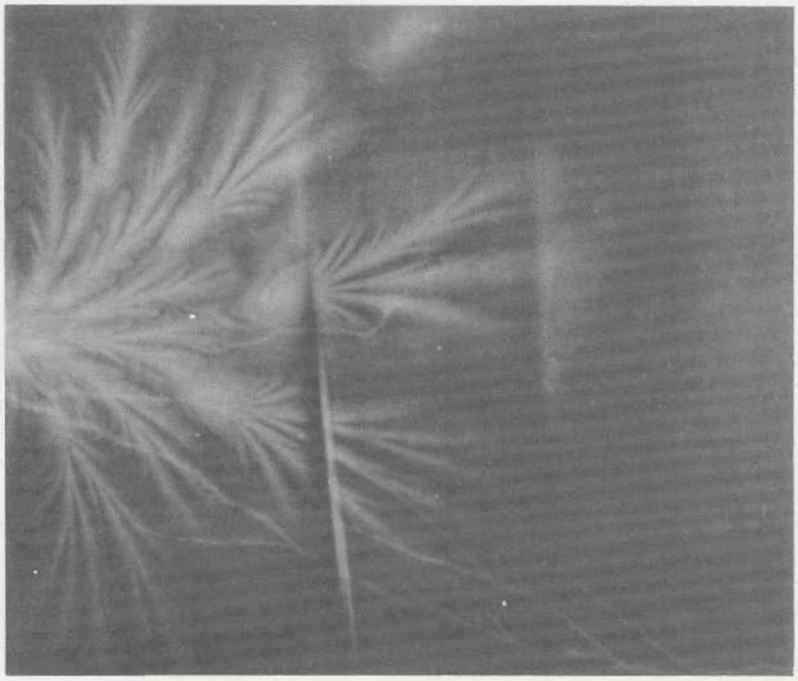

FIGURE 30

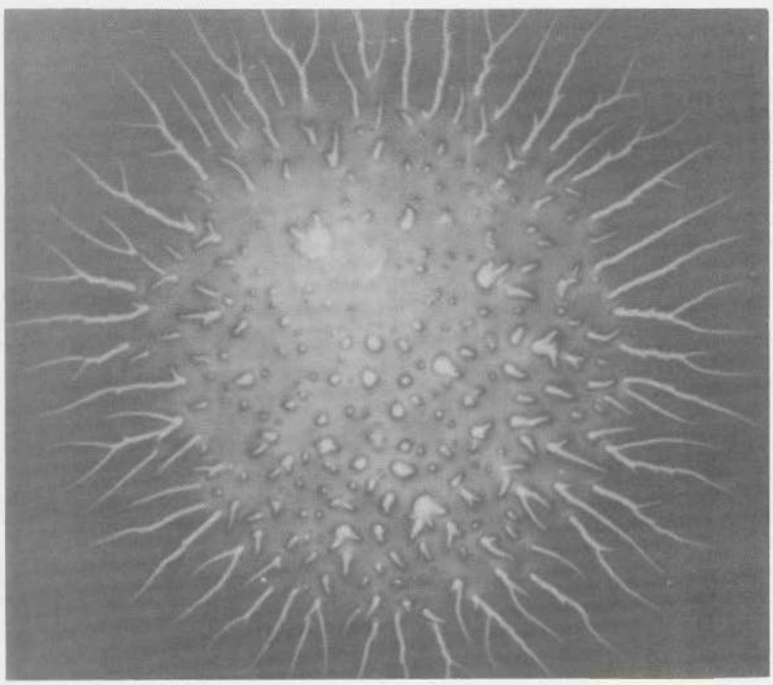

FIGURE 31

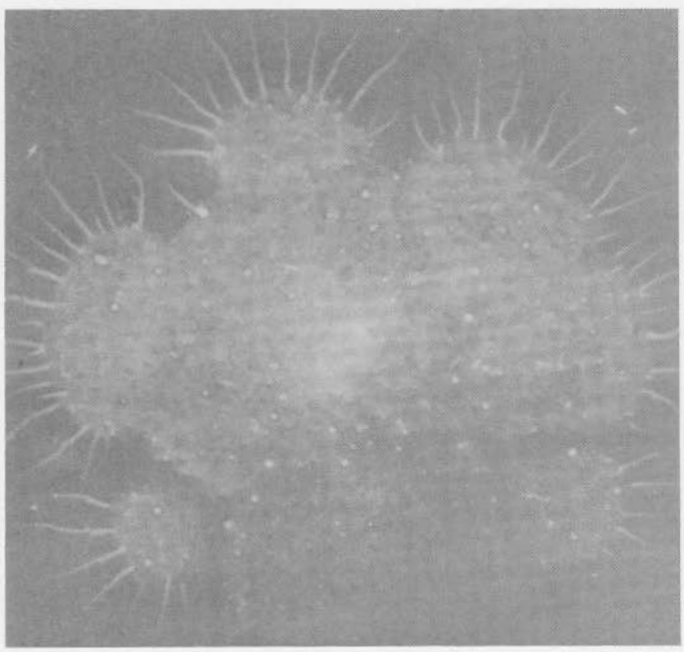

FIGURE 32

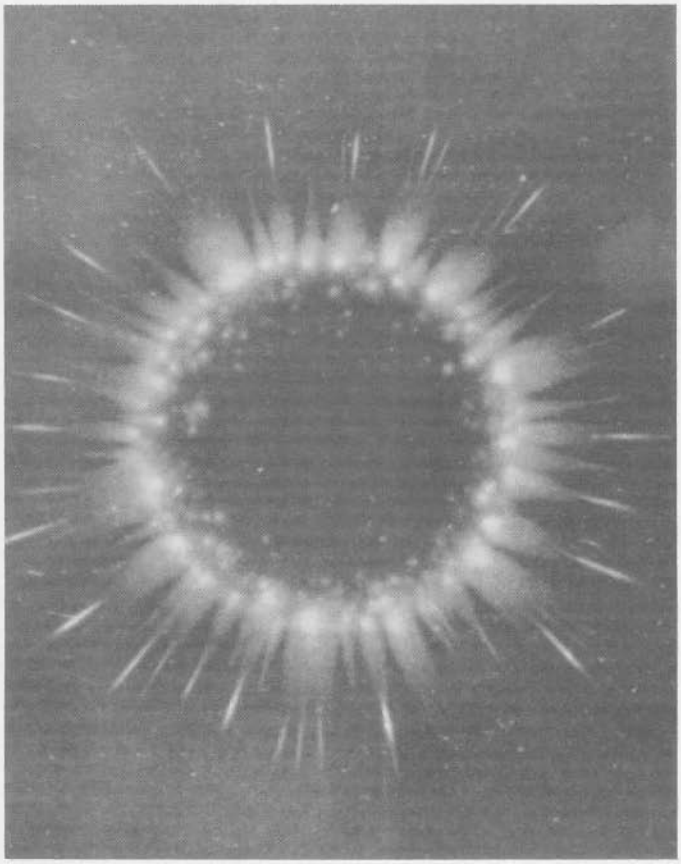

FIGURE 33a

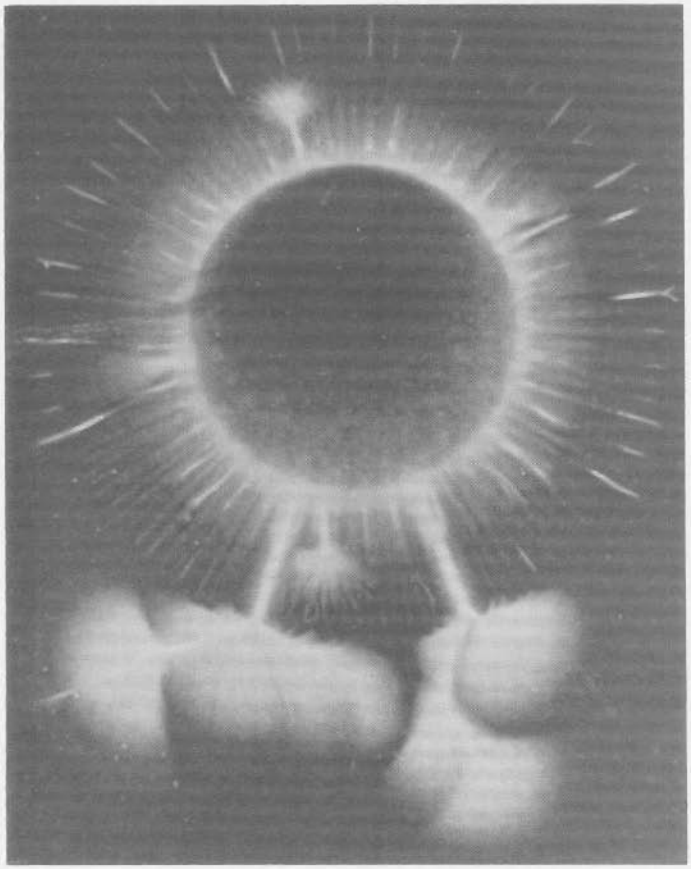

FIGURE 33b

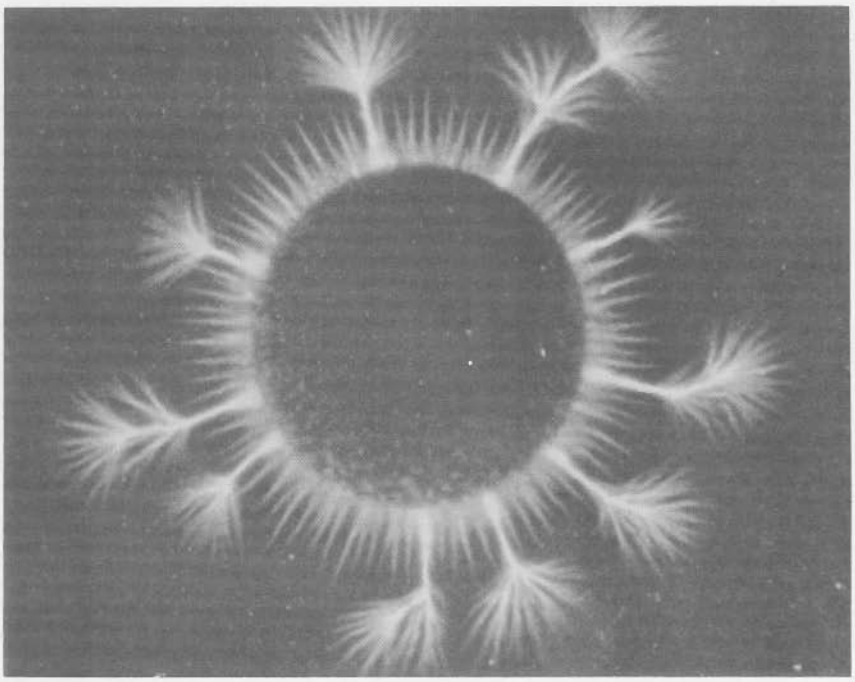

FIGURE 34

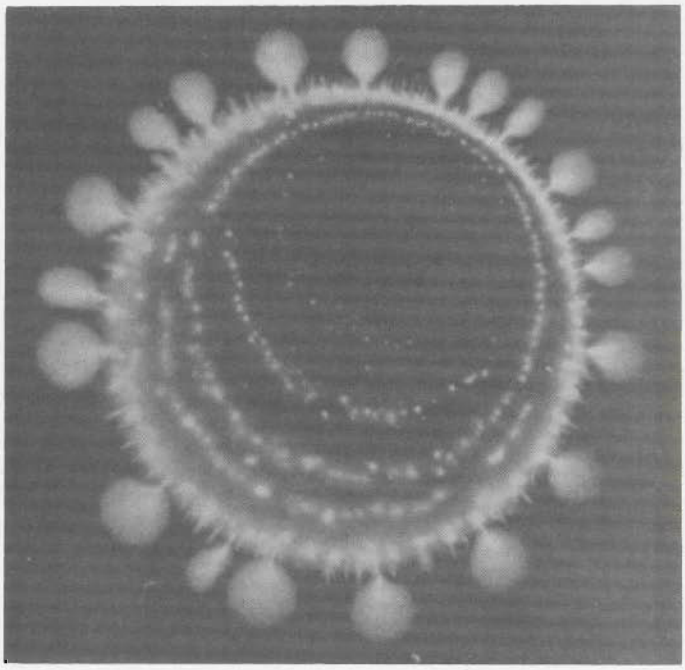

FIGURE 35

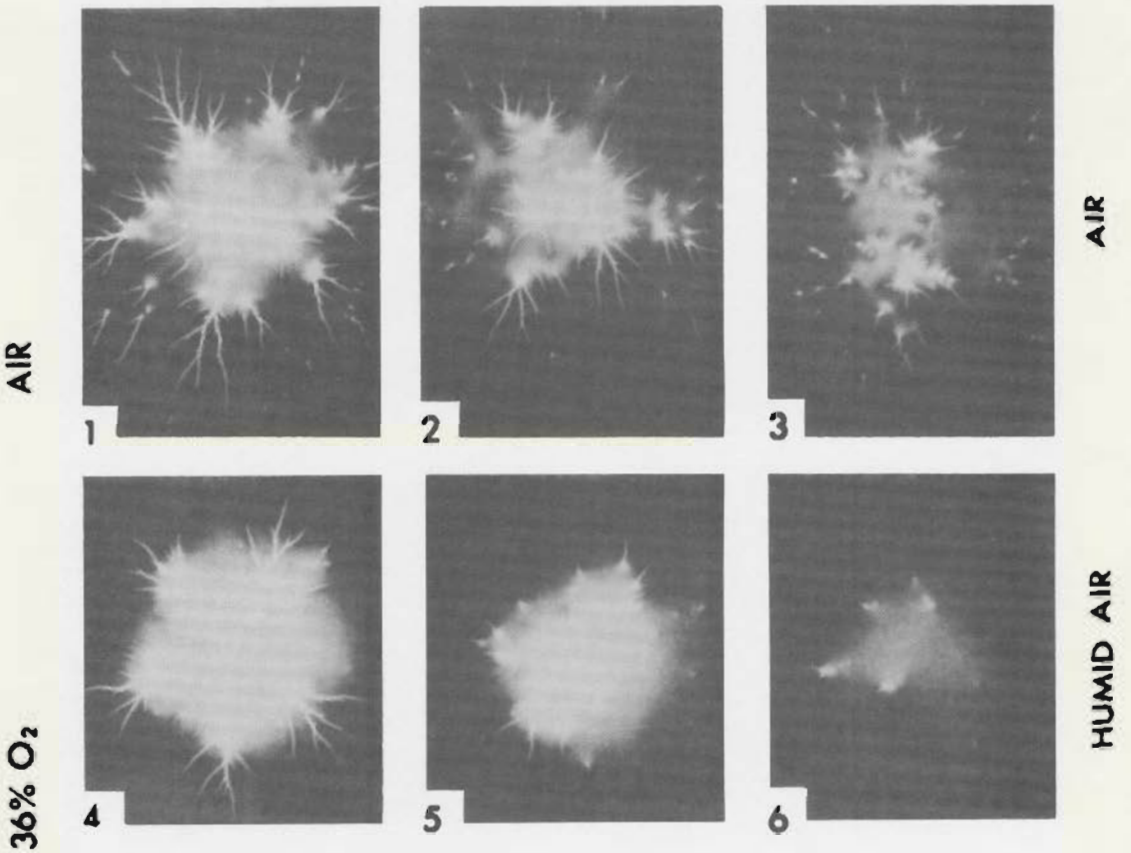

FIGURE 36

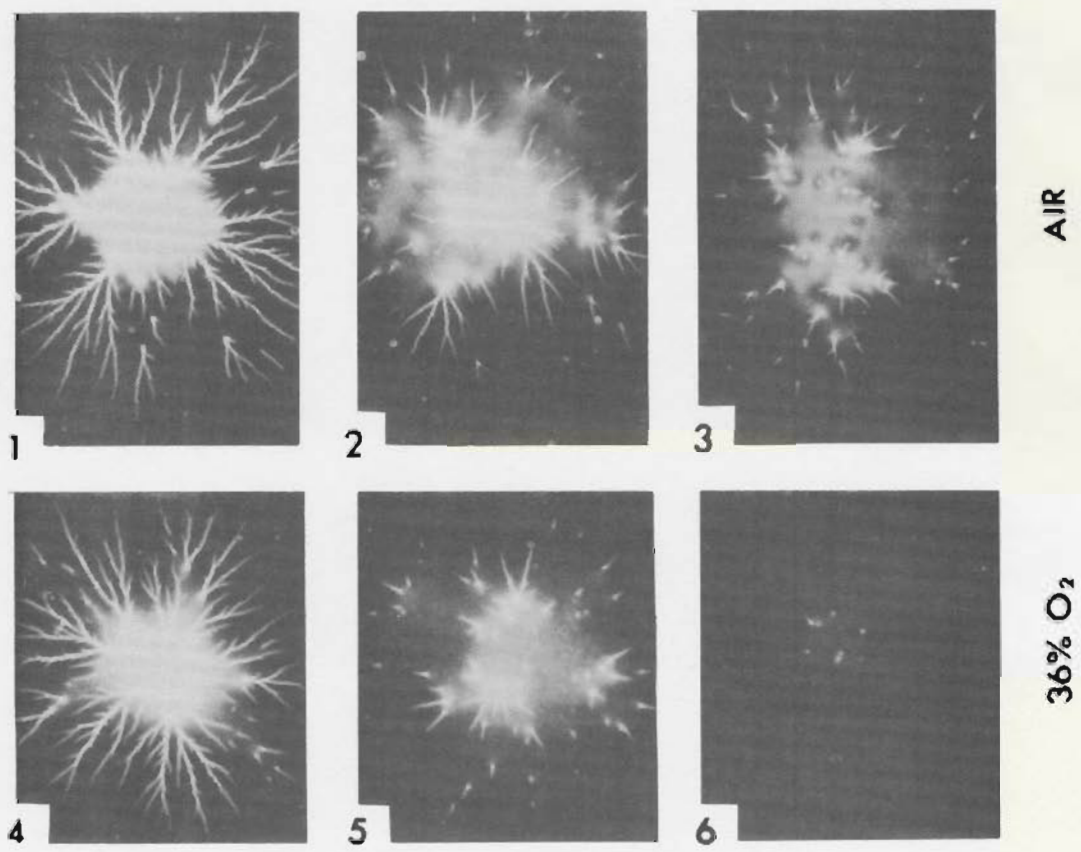

FIGURE 37

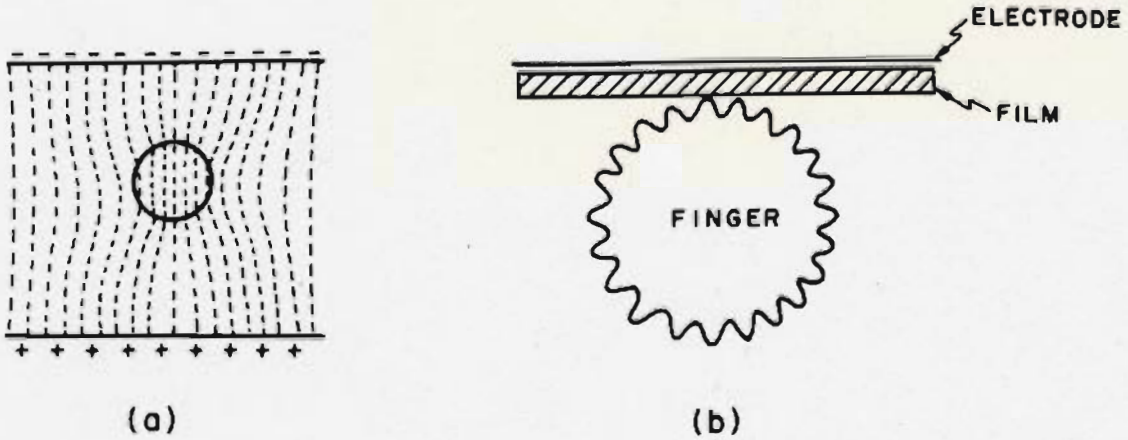

FIGURE 40

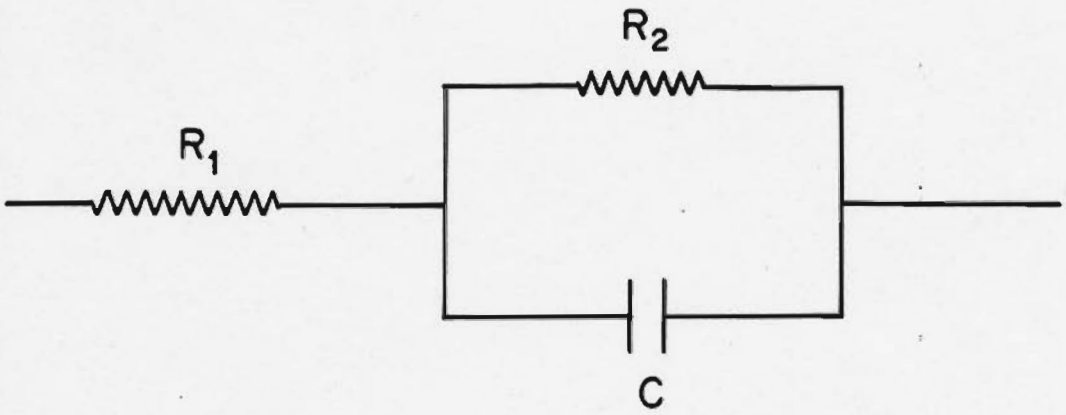

FIGURE 41

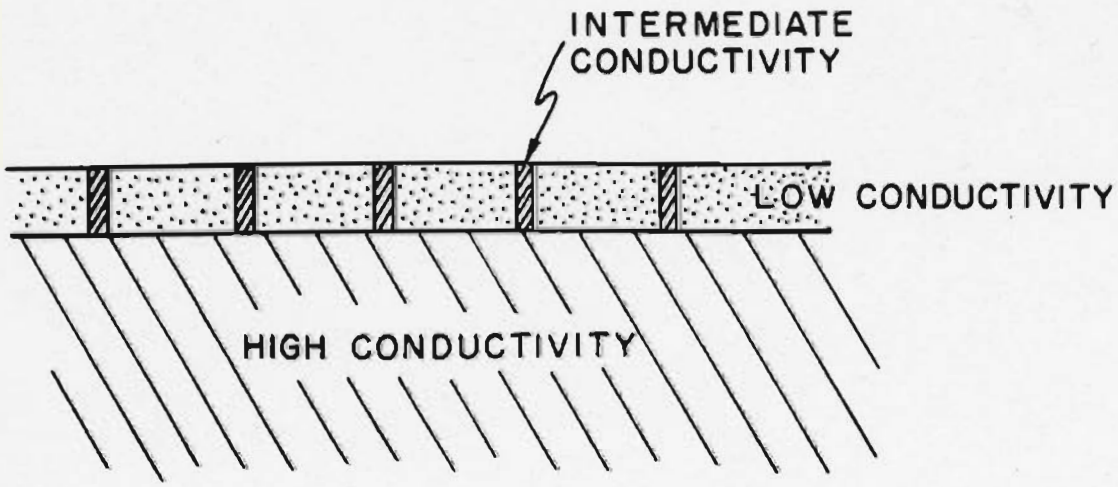

FIGURE 42